Effective Properties of Li-ion Batteries Using a Homogenization Method With Focus on Electrical Conductivity

EFFECTIVE PROPERTIES OF LI-ION BATTERIES USING A MATHEMATICAL HOMOGENIZATION METHOD WITH FOCUS ON ELECTRICAL CONDUCTIVITY

BY

SUBASH DHAKAL, B.Eng.

A THESIS

SUBMITTED TO

THE SCHOOL OF GRADUATE STUDIES

IN PARTIAL FULFILMENT OF THE REQUIREMENTS

FOR THE DEGREE OF

MASTER OF APPLIED SCIENCE

McMaster University

Master of Applied Science (2017) McMaster University

(Mechanical Engineering) Hamilton, Ontario, Canada

TITLE: Effective Properties of Li-ion Batteries Using a Mathematical Homogenization Method With Focus on Electrical Conductivity.

AUTHOR: Subash Dhakal

B.Eng., (Mechanical Engineering)

Tribhuvan University, Kathmandu, Nepal

SUPERVISOR: Dr. Seshasai Srinivasan

NUMBER OF PAGES: xviii, 96

To A.S. and to many fun-filled adventures together in the future...

ABSTRACT

Additives used in the cathode of a Lithium-ion (Li-ion) battery to improve electrical conductivity can negatively impact the ionic conductivity and specific capacity. Therefore, recent focus on the design of Li-ion battery is on the additive-free cathodes. This research work aims to provide a simple rule for the design of cathode microstructure using extensive study of the effect of particle size and volume fraction on effective electrical conductivity. Most design methods used to model the effective transport properties of lithium ion battery electrodes utilize the approximations based on Bruggeman's formula. However, this formula does not consider the microstructure geometry and hence cannot accurately predict the effective transport properties of complicated microstructure like those of Li-ion battery electrodes. In this thesis, based on the principles of mathematical homogenization, an extensive analysis of randomly generated two-phase microstructures idealized for li-ion battery cells is carried out to obtain more accurate estimates of the effective electrical conductivity. To this end, a wide range of values of particle size, volume fraction and conductivity ratios are considered to evaluate the effective conductivity values. From these results, an explicit formulation based on these three parameters to predict the effective conductivity is provided to establish a framework for a simple design rule for additive-free cathode microstructures. Finally, the significance of the microstructural information is highlighted by studying the discharge characteristics of a battery for a theoretical battery model using the Brugemman's formulation as well as the proposed formulation based on the mathematical homogenization technique.

ACKNOWLEDGEMENTS

First and foremost, I would like to thank my supervisor, Dr. Seshasai Srinivasan for giving me the opportunity to work with him and for his incredible support and guidance over the course of this program. I would also like to express my sincerest gratitude towards Dr. Mo Elbestawi and Dr. Mohamed S. Hamed for being part of my committee.

Next, I would like to thank my incredibly supportive family; my dad, mom and my dear brothers. My parents' relentless support for our education and careers has been exemplary.

Finally, I would like to thank the concerned authority of the W. Booth School of Engineering Practice and Technology for providing me access to the graduate studio and computer lab in the Engineering Technology Building (ETB).

NOTATIONS AND ABBREVIATIONS

Nomenclature

σ^*, κ^*	Effective electrical and ionic conductivities, S/m
D^*	Effective diffusion coefficient or Diffusivity, m^2/s
σ, κ	Intrinsic conductivity, S/m
D	Diffusion coefficient or Diffusivity, m^2/s
ε_j	Volume fraction of 'j' phase
γ	Bruggeman's exponent
τ	Tortuosity
r	Domain length normalized particle size
$r_{p/n}$	Actual particle size, μm
N	Number of active-phase particles
h	Conductivity ratio
L	Length of domain

Subscripts

AP	Active particles
E	Electrolyte
p	Positive electrode
n	Negative electrode
s	Separator

Electrochemical Model Symbols

i_s	Current density vector in electrode, A/m^2
i_e	Current density vector in electrolyte, A/m^2
i_m	Local current density in porous matrix, A/m^2
a	Specific surface area, 1/m
c_j	Li+ concentration in phase 'j', mol/m^3
F	Faraday's constant, 96485.33, C/mol
R	Universal gas constant, 8.31 J/mol K
t_+	Transference number of Li+
D_j, σ_j, κ_j	Diffusivity, electrical conductivity and ionic conductivity of j-medium
D^*, σ^*,κ^*	Effective diffusivity, electrical conductivity and ionic conductivity in porous matrix

ε_j	Volume fraction of j- phase
t	Time, s
r	Radius of spherical active particles, m
ϕ	Electric potential, V
T	Temperature, K

TABLE OF CONTENTS

LIST OF FIGURES

LIST OF TABLES

Chapter 1

INTRODUCTION

1.1 Background

Our over-reliance on traditional energy resources like coal and gas to meet the ever-increasing energy demands has led to an increase in atmospheric carbon dioxide levels to an all-time high, resulting in global warming and climate change. Research in the development of clean and renewable energy resources is of prime importance to overcome this problem. One of the key requirements of any renewable energy system, including solar and wind energy is the availability of an efficient energy storage system. Electric vehicle technology development also hinges on the development of high capacity storage systems. Currently, Li-ion batteries are the energy storage systems of choice in electronic devices including laptops, cell phones, etc. as well as in electric vehicles, owing to their high specific energy storage capacity, negligible memory effects, lower self-discharge rate and long cycle rate as compared to other battery technologies [1].

Simulation of electrochemical and thermal properties is arguably the most cost-effective and time-saving tool that can be used in the design of optimal battery systems. This method requires robust and efficient mathematical models that are based on the laws of physics and chemistry. Several methods that vary in differing levels of complexity,

computational cost and accuracy have been used so far. The most widely used models in increasing order complexity are the single-particle model, pseudo-two-dimensional model (P2D) and other molecular/atomistic models [2]. Due to the high-range multi-scale nature of the constituents of the battery ranging from hundreds of micro-meters to a few Nano-meters, it is computationally infeasible to carry out a detailed direct simulation using the properties of all the elements that constitute a Li-ion battery [3]. Hence, it is common practice to model the battery electrodes using effective transport properties of the electrodes which incorporate the information of transport properties of all the constituent phases.

One of the most widely used formula to evaluate the effective properties is the Bruggeman's formula [4]. Although this formula is widely used by the Li-ion battery development community, it is only valid when the conductive phase is continuous and the non-conducting phase consists of uniform-sized spherical particles [5]. Additionally, this formula calculates the effective properties only using the information on volume fraction, ignoring the effects of the microstructure. It is well known that the microstructure of the electrode of a cell can undergo significant changes during a typical operation involving repeated cycling, strongly affecting the effective properties, even though the volume fraction may remain the same. Consequently, the evaluation of effective properties of a complicated microstructure geometry like that of a typical li-ion battery electrode based on this formula is unreliable.

In this research work, a mathematical homogenization method is used to evaluate the effective transport properties of random microstructures with two phases with focus on

effective electrical conductivity. The homogenization method employed in this thesis is inspired by the work done by Gully et al. [3]. In this method, the microstructure information along with the individual phase properties are used to calculate the effective transport properties of complex composite microstructures. Hence, a more accurate representation of the effective properties is obtained for modeling purposes. Based on the calculations using this method, a simple formulation for the evaluation of the effective electrical conductivity using the intrinsic properties of a two-phase electrode microstructure is provided and analysis of the results based on this formula is performed.

1.2 Thesis Scope

This thesis provides a detailed analysis of evaluation of effective properties of the porous positive electrode of Li-ion battery considering two phases, namely, active particles and electrolyte with a focus on the evaluation of effective electric conductivity. Mathematical homogenization method is used to obtain the results which are then compared with the results based on Bruggeman's theory. Results used for evaluation of effective electrical conductivity are used to provide a simple design rule for a two-phase microstructure. Similarly, a brief study of discharge characteristics based on the evaluated effective properties is also discussed.

1.3 Thesis Objectives

The primary objective of the research work is to highlight the importance of considering the microstructure geometry for the evaluation of effective properties using the mathematical homogenization method. In this work, study of the relation between effective electrical conductivity and the microstructure geometry is carried out. In doing so, an empirical relationship between effective electrical conductivity and a given microstructure's defined intrinsic parameters is established.

The specific objectives are as follows:

I. Evaluation of effective electric properties of positive electrode of li-ion batteries considering microstructure geometry information.

II. Study of the effects of particle size, volume fraction and conductivity ratio variation on the effective properties.

III. Comparison of the evaluated effective properties with those evaluated using Bruggeman's formula.

IV. Derivation of an algebraic formulation in order to easily evaluate effective conductivity for an idealized two-phase positive electrode model.

V. Study of the effect of particle size distribution by comparing results based on the calculation of effective properties using mono-modal and bi-modal particle size distributions.

VI. Evaluation of tortuosity of the representative microstructures of electrodes based on the evaluated effective properties.

VII. Study of the effect of the microstructure arrangement on the discharge characteristics using the evaluated effective properties.

1.4 Thesis Organization

This thesis consists of six chapters. A brief description of each chapter is given below:

Chapter 1: The first chapter discusses the background on the research work carried out in this thesis. It also provides a brief discussion on the scope of the thesis, objectives and organization.

Chapter 2: This chapter summarizes the literature review on topics related to Li-ion batteries and their modeling procedure, methods of evaluation of effective properties and mathematical homogenization method.

Chapter 3: The theoretical background behind the mathematical homogenization method to evaluate the effective properties is briefly discussed in this chapter. A brief description of the theory behind the pseudo-two-dimensional (P2D) model is also provided.

Chapter 4: This chapter describes the research methodology employed in this study, with a brief discussion on the process used to generate and define the representative microstructures and the simulation method in COMSOL.

Chapter 5: This chapter consists of all the results for the numerous studies carried out in this research work and the analyses of those results in detail.

Chapter 6: The research findings are briefly summarized in this chapter and discussion on the probable future work is provided.

Chapter 2

LITERATURE REVIEW

This chapter includes a review of literature on the topics related to the design and modeling of Lithium-ion battery and a brief discussion on the effort expended by the research community in this field towards the design of cathode microstructure. A brief review of the world's energy scenario is provided with a note on the importance of development of efficient electrochemical batteries for the development of renewable energy systems and electric vehicles.

2.1 World's Energy Scenario

The total world population which in 2014 was about 7.2 billion is expected to increase to anywhere between 9.6 billion to 12.3 billion by 2100 [6]. With this rapidly increasing population, coupled with the resulting rapid urbanization and industrialization, the demand for energy is ever-growing. Currently, the world relies heavily on fossil fuels to meet most of the energy demands. According to the report on the world's energy scenarios by the World Energy Council (WEC), in 2014 only about 14% of the world's primary energy needs was supplied by renewable energy sources including hydropower and biomass [7]. This share of total energy supply from the popular renewable energy resources is much smaller (~1%) from popular sources including wind and solar [7].

The U.S. Energy Information Agency (EIA) predicts that there will increase by nearly 48% between 2012 and 2040 [7]. With our over-reliance on traditional sources of energy including coal, petrol and diesel, the world is facing significant issues related to air pollution, global warming and climate change. The atmospheric carbon-dioxide (CO_2) concentration as of May, 2017 was at 406.36 ppm; almost 25 percent more than that in 1958 [8]. Increasing concentration of CO_2 has led to an increase in the earth's surface temperature. Consequently, average global temperature in 2016 was 0.99 degree Celsius higher than that in the mid-20^{th} century [9].

With respect to transportation, we still rely heavily on fossil fuels and this sector is a major contributor of greenhouse gases. For example, in 2015, the transportation sector emitted 173 Mt CO_2 in Canada which was about 28% of the total greenhouse gas emissions [10]. Similarly, in the United States, one of the biggest contributors of global greenhouse gases, the transportation sector accounted for 27% of the overall greenhouse gas emissions in 2015 [11].

Use of renewable and clean energy systems can help tackle the problems caused by the excessive use of fossil fuels and provide sustainable alternatives to fossil fuels. These sources of energy are derived directly or indirectly from the sun and are freely available in nature. The major renewable sources of energy are solar, biomass, wind, geothermal and hydropower. These energy resources can be used directly or indirectly for electricity generation, heating and cooling and transportation. According to the report by European Renewable Energy Council (EREC), renewable energy sources in the world can provide 3078 times the world's energy demand [12]. This means that it is possible to depend on

renewable energy resources to meet 100% of the world's energy demands and hence completely phase out fossil fuels in the future.

2.2 Energy Storage Systems

In moving towards this direction, the development of reliable, efficient and cost-effective electric vehicles can help curb the use of combustion engine-based vehicles which are major sources of greenhouse gas emissions. A key requirement for the development of electric vehicles and major renewable energy systems is the availability of efficient and cost-effective energy storage systems. Energy provided by the renewable energy sources like wind and solar is intermittent in nature. Hence, this energy needs to be stored using high capacity storage devices, generally using rechargeable electrochemical battery systems so that it is easily available for use when needed.

There are different types of energy storage systems in which energy can be stored in the form of compressed air, gravitational(potential) energy, thermal energy, hydrogen (fuel cells) and chemical energy (batteries) [13]. Among these, the electrochemical batteries, which covert chemical energy to electrical energy without producing harmful emissions or noise are the most popular systems. Other advantages of such batteries are their portability and good energy density. The most widely used electrochemical energy storage systems are the rechargeable batteries such as Lead-acid, Nickel-Cadmium (NiCd), Nickel-Metal Hydride (NiMH) and Li-ion batteries among others.

2.3 Lithium-ion Batteries

Li-ion batteries are the most widely used rechargeable batteries in electrical vehicles and consumer electronics owing to their high specific capacity, negligible memory effects, lower self-discharge rate and long cycle rate as compared to other rechargeable battery systems [14-16].

2.3.1 Composition

The key constituents of a typical Li-ion battery are the two electrodes (cathode and anode), electrolyte and a separator as shown in Figure 2.1. There are several types of Li-ion batteries in use in market currently and each has its own chemistry, performance and cost characteristics.

In general, the positive electrode (cathode) consists of a lithium metal oxide ($LiFePO_4$, $LiMn_2O_4$ etc.) and the negative electrode (anode) is made of up graphite or other carbon materials. Electrolyte used in these batteries is made of lithium salts ($LiPF_6$, $LiBF_4$, etc.) in an organic solvent. The separator is usually made up of a permeable membrane and allows the transport of lithium-ions through it whilst blocking the passage of electrons to avoid short-circuiting.

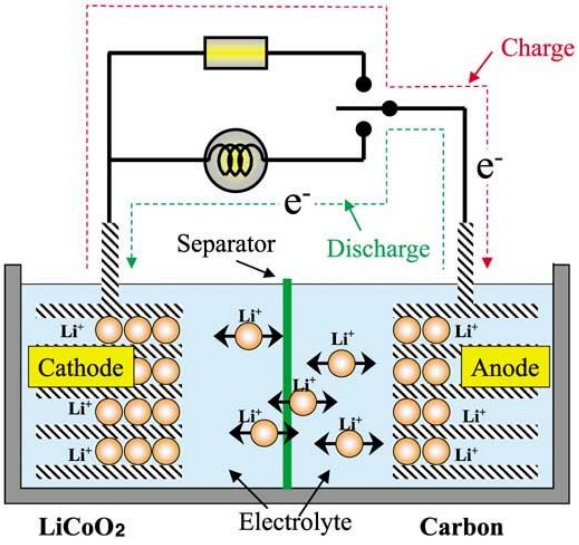

Figure 2.1: Schematic diagram of Li-ion battery. [17]

The exact composition (i.e. fraction and type of material) of any Li-ion battery is determined by the battery chemistry. This battery chemistry is in turn determined based on the desired battery performance for the intended application. The constituents of a typical Li-ion battery used in the electric vehicles (EVs) are given in Table 2.1. The values are

Table 2.1: Percentage mass of battery occupied by major components of a typical $LiMn_2O_4$ electrode-based electric vehicle battery. Data are extracted from the report by Argonne National Laboratory. [18]

Component	**% Mass of battery**
Active material ($LiMn_2O_4$)	33
Graphite/Carbon black	12
Binder (PVDF)	2.5
$LiPF_6$	1.8
Ethylene Carbonate (EC)	5.3
Dimethyl Carbonate (DMC)	5.3
Separator (Polypropylene & Polyethylene)	1.99

percent mass of battery and the total cell mass is 80-90% of the total battery mass [18]. Graphite or Carbon black, which is the main material in the anode is also added to cathode in order to increase the electronic conductivity and occupies nearly 12% of the battery mass. Rest of the mass of the battery is occupied by copper (11%) and aluminum (19%) which are the current collectors and other parts including thermal insulation and electronic parts [18].

2.3.2 Working Principle

The working principle of this type of battery is based on the Li-ion insertion and extraction from the negative electrode during charge and discharge cycles respectively. As Li-ions move across the electrodes, current passes through the outer circuit (see Figure 2.1). During the discharge cycle, lithium ions are released from the negative electrode towards the positive electrode. Similarly, during the charge cycle, these ions get extracted from the positive electrode and are stored in the negative electrode. The net electrochemical reaction taking place in a typical conventional Li-ion battery with the positive electrode composed of $LiFePO_4$ is given below [19]:

$$FePO_4 + Li^+ + e^- \underset{\text{Charge}}{\overset{\text{Discharge}}{\rightleftharpoons}} LiFePO_4$$

2.3.3 Properties of Constituent Phases

Each of the constituent phases of electrodes has its own intrinsic property. The values of conductivity (ionic and electrical), diffusivity and thermal conductivity define the behavior of each phase. Accurate estimates of these values are extremely important for the design of the battery as a whole. It is however extremely difficult to ascertain the exact value of the transport properties of each constituent phase because of the complicated microstructure and the ever-changing physical conditions inside the battery at different cycles of operation.

Park et al. [20] provided a comprehensive review of the conduction phenomena in Li-ion batteries using information obtained from experimental, theoretical and numerical studies. Similarly, Valøen et al. [21] carried out a study of the transport properties $LiPF_6$ used in Li-ion battery electrolytes. Information on the conductivity and li-ion diffusivity

Table 2.2: Transport properties of popular electrode and electrolyte materials.

Component	**Material**	**D** ($cm^2\ s^{-1}$)	**σ** ($S\ cm^{-1}$)	**κ** ($S\ cm^{-1}$)
Cathode	$LiCoO_2$	10^{-10} to 10^{-8} [20]	10^{-4} [20]	-
	$LiMn_2O_4$	10^{-11} to 10^{-9} [20]	10^{-6} [20]	-
	$LiFePO_4$	10^{-14} to 10^{-15} [20]	10^{-9} [20]	-
Anode	Graphite	10^{-14} to 10^{-8} [20]	10^{2} to 10^{4} [20]	-
Electrolyte	$LiPF_6$ (EC: DMC)	10^{-6} to 10^{-7} [21]	-	10.7 [20]

values of some of the widely used materials in Li-ion batteries is presented in Table 2.2. The values of these transport coefficients change with temperature and concentration giving a wide range of possible values and can also vary based on the technique used to calculate them.

2.4 Modeling of Lithium-ion Battery

In this section, a brief discussion of the popular methods used to model the battery is provided. Although the focus of the discussion will specifically be on the Li-ion battery electrode modeling methods, it is important to note that these methods are applicable for other porous systems as well.

There are several methods for battery modeling including behavioral, equivalent-circuit and electrochemical models. Behavioral models utilize empirical functions to determine terminal voltage whereas the equivalent-circuit models use components like resistors and capacitors to represent battery's behavior. Discussion of these models is out of scope of this thesis. Hence, only a brief discussion of the most widely used electrochemical models (ECMs) is provided here. These physics-based models are complex and computationally expensive. However, since these ECMs delve into the battery processes in great detail, they are the most accurate class of models available [22]. The choice of a particular model among the available ECMs depends on the trade-off between the complexity, cost and time required for modeling. Following sub-sections provide a brief review of the Single Particle Model and Pseudo-two-dimensional models.

2.4.1 Single Particle Model

The Single Particle Model is the most simplistic electrochemical model in which the diffusion and intercalation phenomena are modeled within a single electrode particle. These phenomena are only considered inside the single particle but neglected in the solution phase between different particles making this a fast and computationally inexpensive but less accurate and robust model as compared to the other models [22-23]. In this model, the governing equations are simplified by using one Partial Differential Equation (PDE) and one algebraic equation to represent the complete ECM of five PDEs and one algebraic equation [24]. A simple schematic representation of this model is presented in Figure 2.2. As shown in the schematic diagram, in this model, each of the electrodes is represented by a single particle.

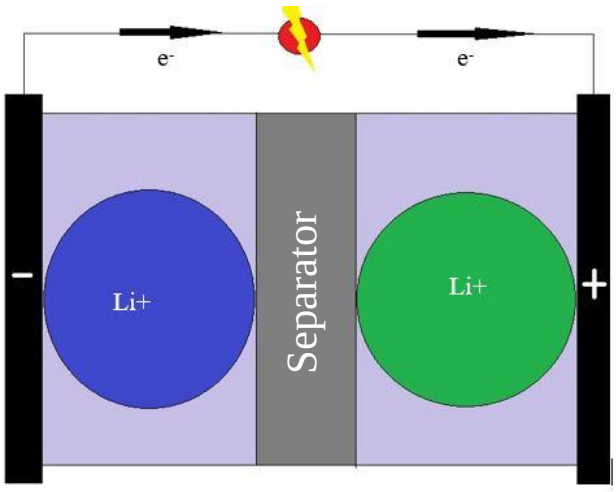

Figure 2.2: Schematic diagram of Single Particle Model (SPM). Each electrode is represented by one particle.

2.4.2 Pseudo-two-dimensional (P2D) Model

The pseudo-two-dimensional (P2D) model, which was first proposed by Doyle et al. [25], is one of the most used electrochemical models because it provides a good bridge between the choice of a more comprehensive model than the simplified SPM model and a more computationally inexpensive model than the multi-scale multi-physics models. This model describes the internal behavior of the Li-ion battery cell and consists of the two electrodes, a separator and current collectors [23]. It is based on the combination of the porous electrode theory developed by Newman et al. [26] and the concentration solution theory [27]. In this model, the electrodes are considered to be composed of a porous matrix. The active particles are assumed to be spherical in shape and the transport process is assumed to be dominant in a single direction (x-axis) making it suitable to be modeled using a 1D-model [27]. A brief discussion of the governing equations used in this model is provided in Chapter 3. Application of this method in conjunction with the homogenization method is presented in Chapter 5.

2.4.3 Multi-physics Models

A lot of research has taken place with a focus on the extension of the P2D model and on more robust multi-scale and multi-dimensional multi-physics models which incorporate the coupled electrochemical-thermal properties to more accurately describe the complex processes taking place inside the Li-ion cell [27]. However, these are very difficult to implement with added computational cost and time. Furthermore, a lot more research is

required to fully understand and implement these models. For more information on the state-of-the-art of research on multi-physics models, the reader is referred to the work by Ramadesigan et al. [23].

2.5 Design of Lithium-ion Battery Positive Electrodes

The cathode or positive electrode of a Li-ion battery consists of three distinct phases viz. active particles, polymer binder (doped with conductive carbon particles) and electrolyte, as shown in Figure 2.3. The active material, which is the principle constituent, acts as a reservoir for the storage of lithium ions. Binders and carbon additives are the inactive materials in the cathode. The binder is used in the electrode to bind the active materials with the conductive additive phase. The conductive additive is used in order to increase the overall conductivity of the bulk composite [28].

Energy density, rate capability and consequently the cost of a Li-ion battery is dependent upon the porous cathode [29]. Hence, the design of cathode is a very important process which determines the overall performance of a Li-ion battery. One of the most important aspects to consider while designing the cathode is to obtain an optimal design of the microstructures considering the trade-off between electrical and ionic conductivities [29]. As discussed earlier, the carbon additives are added to improve the electrical conductivity by increasing the electronic pathways. However, the addition of these additives can obstruct the pathways for the transport of ions [29]. Therefore, an optimal

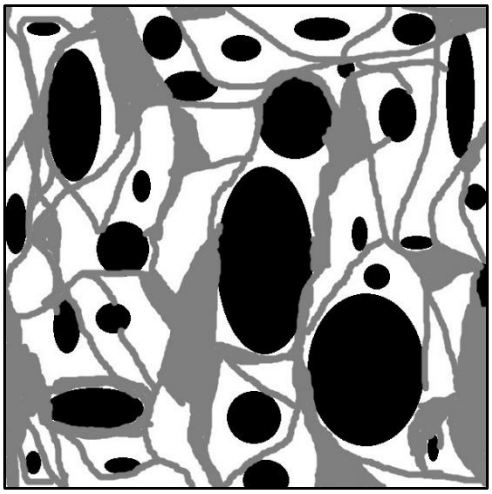

Figure 2.3: Schematic representation of Li-ion battery cathode in microscale showing electrolyte (white), active particles (solid black shapes) and binders (gray strands).

trade-off between the electronic and ionic transport is vital for an improved performance of the cathode and consequently the Li-ion cell.

2.5.1 Conductivity Enhancement of Cathode

The improvement of the conductivity of cathode materials has so far only been possible using two processes: a) inclusion of conductive additives and b) reduction of particle size [20]. Typical materials used as conductive additives include carbon black and graphite ultra-fine carbon (UFC) suspensions [30]. Use of these additives has been shown to increase cyclability and measurable increase in conductivity [30]. A key factor to consider while using the additives to increase the conductivity is the ratio of PVDF (poly-vinylidene fluoride) , the most commonly used binder to carbon black. Chen et. al [30] presented this ratio as the most significant factor affecting conductivity.

Although the addition of carbon additives can help improve the electrical conductivity, it can also impede ionic conductivity. Also, these additives occupy anywhere between 10-40% of the weight of the electrode [31]. These additives are used to increase electrical conductivity and to bind the active particles with the conductive fillers but do not actually participate in electrochemical reactions. Consequently, the specific energy capacity of the cell, one of the key parameters in battery selection, is limited due to the use of additives. One other issue with the use of the additives is the difficulty that they create in the modelling of the transport of li-ions and electrons through the composite. Therefore, one of the key areas of focus in the research community for the improvement of Li-ion batteries is on the design of conductive additive-free electrodes. Ha et al. [31] introduced a general procedure for the fabrication of binder and carbon-additive free high performance Li-ion battery electrode using Nanoparticles. They also provided a framework for the study of the influence of active particle size on overall cell capacity without the interference of the additives.

2.5.2 Influence of Active Particles Size and Distribution

The size and distribution of active particles can also have a significant impact on the performance of the cathode. It has been found that the reduction in the size of active particles, on a micro-scale, significantly increases the rate capability of Li-ion batteries [32]. Similarly, use of Nanomaterials for battery electrodes has been found to boost the electrochemical properties of the battery by reducing diffusion or transport distance of the

ions and electrons and enhancing the reversible Li-ion intercalation process [32]. Therefore, smaller particle sizes are generally desired. However, since the Nano-sized particles are highly reactive due to their larger surface area, safety and stability become major issues over their long life-cycles [33]. Hence, control of the size of active particles is a very important part of design of cathodes of Li-ion batteries.

Yu et al. [34] showed that for Li_2MnO_3-based materials, smaller particle size samples provide much larger charge-discharge capacity compared to their larger sized counterparts. Similarly, Yabuuchi et al. [35] used Li_2MnO_3-based lithium-excess electrodes used micro-sized and Nano-sized particles to study the effect of particle size on electrode performance and phase transition behavior. They found that the initial discharge capacity significantly increases when the Nano-sized particles (<100 nm) are used as compared to the micro-meter sized particles (>1μm). However, they also reported that this high initial discharge capacity obtained using Nano-sized particles quickly decreases with increased cycling and the resulting phase transition causes a change in the voltage profile.

In addition to the size of active particles, particle polydispersity also plays a crucial role in the porous cathode microstructure of Li-ion batteries [36]. By modifying the P2D model, Taleghani et al. [37] showed that the volume fraction of particles of different sizes in a multi-modal particle size distribution has a very significant impact on cell capacity, voltage and specific power. Garcia et al. [38] examined the sensitivity of the electrochemical performance of a $Li_yC_6|Li_xMn_2O_4$ battery system as a function of particle size by employing a finite element model to study arbitrary two-dimensional microstructures of electrodes. They found that a homogeneous, small, well-dispersed particle size distribution yields

higher power densities and better utilization of the active material particles. With the help of three-dimensional X-ray tomography data of a $LiMn_2O_4$ electrode, Chung et al. [39] carried out electrochemical simulations of computer-generated microstructures to study the effect of particle size polydispersity in Li-ion batteries . They found that clusters of small particles provide more lithium intercalation as compared with the regions with clusters of larger particles. Additionally, they also highlighted that monodispersed particle sized electrodes, because of their high surface area to volume ratio, provide more power density for high discharge rate applications. For high discharge applications, some of the larger active particles become underutilized because of higher rate of reaction of the smaller particles. Also, for low discharge rate applications, poly-dispersed distribution provides more specific energy as compared to monodispersed distribution [39].

2.6 Evaluation of Effective Properties of Cathodes

Enhancement of the capacity in the modern lithium ion batteries has been possible in part because of the increase in ionic and electronic conductivities of the electrodes through the use of better materials [20]. In order to effectively model a Li-ion battery, an accurate description of the key transport properties viz. diffusivity and ionic, electronic and thermal conductivities is desired. In this section, a brief overview of the research on the evaluation of the transport properties of Li-ion battery cathodes is provided.

Bruggeman's formula is the most popular approximation method used extensively to evaluate the effective transport properties [4]. However, because of its inability to

incorporate the information related to microstructure geometry, predictions based on this formula are unreliable [3,5,36]. A lot of research work has been undertaken to improve the accuracy of this formula. Vadakkepatt et al. [40] used Finite Volume Method (FVM) to study the actual microstructures of a Li-ion battery to show that Bruggeman's formula for evaluating the thermal conductivity needs recalibration to improve its accuracy. Similarly, Yan et al. [41] employed a three-dimensional model utilizing experimental electrode microstructures without using the Bruggeman's formula to evaluate the effective properties and were able to obtain more accurate results of battery performance. Samantray et al. [42] proposed formulations for the evaluation of the effective thermal conductivity for two-phase materials and found that their predictions were much closer to the experimental results than the oft-used Bruggeman's formula.

The focus of this research work is on the evaluation of the effective electrical conductivity of Li-ion battery cathodes using mathematical homogenization method. It is vital to accurately predict the effective electrical conductivity value of an electrode for optimal design of a Li-ion battery [43,44] and this is a topic of great interest in the Li-ion battery research community. For instance, Hutzenlaub et al. [45] reconstructed a $LiCoO_2$ cathode and carried out numerical simulation to evaluate the effective electrical conductivity in all three spatial directions. Similarly, Chen et al. [46] provided a technique for the optimal design of Li-ion battery cathode by using predictive methods to determine both ionic and electrical conductivities.

Chapter 3

THEORETICAL BACKGROUND

This chapter describes the theoretical background on the mathematical homogenization method which is used to evaluate the effective transport properties. It also includes a brief discussion on the underlying theory of the pseudo-two-dimensional electrochemical model used for calculation of the discharge characteristics.

3.1 Mathematical Homogenization Method

The mathematical homogenization method used in this thesis is based on the work by Gully et. al. [3]. A brief description of the derivation of the equation to be used for the evaluation of effective transport properties of porous battery electrode material is provided in this section. The calculations based on this homogenization technique allows for the evaluation of effective transport properties taking into consideration the microstructure geometry information. Although the description provided here is based on the evaluation of effective electrical conductivity, derivations for other effective properties including effective diffusivity , ionic and thermal conductivity are mathematically identical to this description [3,47].

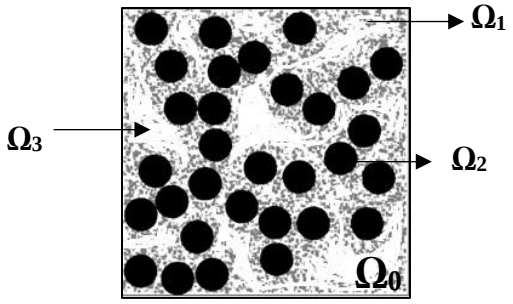

Figure 3.1: Schematic representation of the microstructure domain Ω_0.

Assumptions regarding the microstructure domain Ω_0 shown in Figure 3.1 are provided below:

a) Ω_0 is periodic in all three directions.

b) Ω_0 is a union of three subdomains Ω_1, Ω_2 and Ω_3 which represent the three distinct phases, i.e., $\Omega_0 = \Omega_1 \cup \Omega_2 \cup \Omega_3$.

c) Each of the phases Ω_j, j=1, 2, 3, is isotropic.

d) The individual phases are characterized by non-zero conductivity coefficients σ_j, (j=1,2,3), such that

$$\sigma(\mathbf{x}) = \sigma_1\chi_1(\mathbf{x}) + \sigma_2\chi_2(\mathbf{x}) + \sigma_3\chi_3(\mathbf{x}) \tag{3.1}$$

$$\chi_j(\mathbf{x}) := \begin{cases} 1 & \mathbf{x} \in \Omega_j, \\ 0 & \mathbf{x} \notin \Omega_j \end{cases} \tag{3.2}$$

where χ_j is the characteristic function of the j-th phase (": =" means "equal by definition").

The Ohm's law can be written as

$$\mathbf{J}(\mathbf{x}) = \sigma(\mathrm{x})\mathbf{E}(\mathbf{x}) \tag{3.3}$$

where **J** and **E** represent the electric current and electric field respectively while σ(x) is defined in Equation (3.1). It should be noted that this electric current is due to the transport of electrons and doesn't account for the ionic current induced by the transport of chemical species in electrochemical systems. The electric field can simply be stated as the negative gradient of the electric potential. Also, there are no sources or sinks of charge within the material. Hence, we can write

$$\boldsymbol{\nabla} \times \mathbf{E}(\mathbf{x}) = \mathbf{0} \quad \text{and} \quad \boldsymbol{\nabla}.\mathbf{J}(\mathbf{x}) = 0. \tag{3.4}$$

Let

$$\langle \mathbf{E} \rangle = \mathbf{e}_k, \tag{3.5}$$

where $\mathbf{e}_k$ is a unit vector in the k-th direction for k =1,2,3. We can re-write Ohm's law as

$$\langle \mathbf{J} \rangle = \sigma^* \langle \mathbf{E} \rangle \tag{3.6}$$

Here, $\langle \cdot \rangle$ is the spatial average over a periodic microstructure Ω_0. Following the mathematical transformations described by Gully et al.[3], we can write the electric field **E** as

$$\mathbf{E} = [\mathbf{I} + s_1^{-1}\boldsymbol{\Gamma}\chi_1 + s_2^{-1}\boldsymbol{\Gamma}\chi_2]^{-1}\mathbf{e}_k \tag{3.7}$$

where

$$s_1^{-1} := 1 - \sigma_1/\sigma_3 \quad \text{and} \quad s_2^{-1} := 1 - \sigma_2/\sigma_3 \tag{3.8}$$

Here **I** represents the identity operator. Also for arbitrary vector field **z**, the operator **Γ** is defined as

$$\boldsymbol{\Gamma}\mathbf{z} := \boldsymbol{\nabla}\,(-\Delta)^{-1}\boldsymbol{\nabla}.\,\mathbf{z} \tag{3.9}$$

Here, Δ is the Laplacian operator. On denoting $\sigma^* = [\sigma^*]_{kk}$ as the kk-th component of the effective conductivity tensor, it can be shown that:

$$[\sigma^*]_{kk} = \sigma_3[1 - \langle e_k^T(\mathrm{s}_1^{-1}\chi_1 + \mathrm{s}_2^{-1}\chi_2)[\mathbf{I} + \mathrm{s}_1^{-1}\boldsymbol{\Gamma}\chi_1 + \mathrm{s}_2^{-1}\boldsymbol{\Gamma}\chi_2]^{-1}\mathbf{e}_\mathrm{k}\rangle] \tag{3.10}$$

As mentioned earlier, this derived equation is mathematically identical for all other effective transport properties. Here, microstructural geometric information can be imported for each of the three phases as functions of the parameters χ_1, χ_2 and χ_3. Similarly, the information of intrinsic conductivity of individual phase of a given microstructure is contained in the ratios given by s_1 and s_2 as described earlier.

Based on Equations (3.7) and (3.9), the electric field **E** can be expressed as

$$\mathbf{E} + \boldsymbol{\nabla}\,(-\Delta)^{-1}\boldsymbol{\nabla}.\,[(\mathrm{s}_1^{-1}\chi_1 + \mathrm{s}_2^{-1}\chi_2)\mathbf{E}] = \mathbf{e}_\mathrm{k} \tag{3.11}$$

Upon introducing an auxiliary potential variable given by

$$\psi := (-\Delta)^{-1}\boldsymbol{\nabla}.\,[(\mathrm{s}_1^{-1}\chi_1 + \mathrm{s}_2^{-1}\chi_2)\mathbf{E}] \tag{3.12}$$

we can re-write Equation (3.11) in the form of following system of equations:

$$\boldsymbol{\nabla}.\,[(-1 + \mathrm{s}_1^{-1}\chi_1 + \mathrm{s}_2^{-1}\chi_2)\boldsymbol{\nabla}\psi] = \boldsymbol{\nabla}.\,[(\mathrm{s}_1^{-1}\chi_1 + \mathrm{s}_2^{-1}\chi_2)\mathbf{e}_\mathrm{k}] \tag{3.13}$$

$$\mathbf{E} = \mathbf{e}_\mathrm{k} - \boldsymbol{\nabla}\psi. \tag{3.14}$$

Numerical solution of this system of equations subject to periodic boundary conditions based on the stated assumption provides the required effective electrical conductivity for a porous battery electrode. The effective electrical conductivity tensor based on the derived equations can be simply stated as follows:

$$[\sigma^*]_{kk} = \sigma_3\left[1 - \langle \mathbf{e}_k^T(s_1^{-1}\chi_1 + s_2^{-1}\chi_2)\mathbf{E}\rangle\right]. \quad (3.15)$$

Although three distinct phases have been used for this formulation, only two distinct phases have been considered in this study. However, this formulation can be easily modified during implementation in COMSOL to evaluate the desired two-phase effective properties.

3.2 Electrochemical model

This section provides a brief discussion on the governing equations for the P2D electrochemical model discussed in section 2.4. The governing mathematical equations of this P2D model can be separately represented in terms of the two electrodes and the separator regions. The equations presented here are based on the work by Doyle et al. [25] . The values of effective properties given in all the equations are usually corrected using Bruggeman's formula as discussed in Chapter 2. Information on the symbols used in this section are provided separately under *Notations and Abbreviations*.

3.2.1 Electrode region

The positive and negative porous electrode regions consist of both the electrode and electrolyte phases. Based on Ohm's law, the current density vector, $\mathbf{i_s}$, in the electrode phase of the porous electrode regions can be stated as:

$$\mathbf{i_s} = -\sigma_s^* \nabla \emptyset_s \, . \tag{3.16}$$

Similarly, the conservation of lithium ions in the case of electrodes can be stated as

$$\frac{\partial c_s}{\partial t} = \nabla . (D_s \nabla c_s) \tag{3.17}$$

with boundary conditions given by:

$$\left.\frac{\partial c_s}{\partial t}\right|_{r=0} = 0 \, , \qquad -D_s \left.\frac{\partial c_s}{\partial t}\right|_{r=r_p} = i_m \tag{3.18}$$

The gradient of Equation (3.18) can be calculated in COMSOL in cartesian , cylindrical or spherical co-ordinates depending upon whether the particles are assumed to be flakes , rods or spheres , respectively [48].

3.2.2 Electrolyte region

The current balance in the electrolyte phase of porous electrode regions can be written as:

$$\frac{1}{F} \nabla . i_e = a i_m . \tag{3.19}$$

The current density vector, $\mathbf{i_e}$, in the electrolyte is given by:

$$i_e = -\sigma_e^* \nabla \emptyset_e + \left(\frac{2 k_e^* R T}{F}\right)\left(1 + \frac{\partial \ln f}{\partial \ln c_e}\right)(1 - t_+) \nabla \ln c_e \tag{3.20}$$

Similarly, the conservation of lithium ions in the electrolyte phase is given by:

$$\varepsilon_e \frac{\partial c_e}{\partial t} = \nabla.(D_e^* \nabla c_e) - \frac{i_e \cdot \nabla t_+}{F} + a i_m (1 - t_+) \tag{3.21}$$

The solid phase particles in this study are assumed to be spherical. For spherical particles, the interfacial surface area can calculated as [48]:

$$a = \frac{3\varepsilon_s}{r}. \tag{3.22}$$

If a multi-sized particle model like a three-particle size model is to be used instead of the original single-particle model, the P2D model needs to be extended to include the corresponding differences in volume fraction and particle size. Lee et. al [49] provide an extended P2D model using three particle sizes in which the solid phase volume fraction is divided into three different parts to represent small, medium and large particles such that :

$$\varepsilon_s = (\varepsilon_{s,L} + \varepsilon_{s,M} + \varepsilon_{s,S})\varepsilon_s . \tag{3.23}$$

The total specific surface then becomes:

$$a = a_L + a_M + a_S . \tag{3.24}$$

Again, for spherical particles, the individual specific surface areas can be written as:

$$a_L = \frac{3\varepsilon_{s,L}}{r_L}, a_M = \frac{3\varepsilon_{s,M}}{r_M} \text{ and } a_S = \frac{3\varepsilon_{s,S}}{r_S}. \tag{3.25}$$

3.2.3 Butler-Volmer Equation

The Bulter-Volmer kinetics equation links the electrolyte and electrode phase and is given by:

$$i_m = i_o \left(\exp\left(\frac{\alpha_a F \eta}{RT}\right) - \exp\left(\frac{-\alpha_a F \eta}{RT}\right) \right) \tag{3.26}$$

The value of coefficient i_o can be written as:

$$i_o = F\,(k_c)^{\alpha_a}(k_a)^{\alpha_c}\,(c_s)^{\alpha_c}\left(\frac{c_e}{c_{e,ref}}\right)\left(c_{s,max} - c_s\right)^{\alpha_a} \tag{3.27}$$

The overpotential, η , which drives the electrochemical reaction can be written as:

$$\eta = \phi_s - \phi_e - E_{eq} \tag{3.28}$$

Chapter 4

RESEARCH METHODOLOGY

In this chapter, the methods used to generate idealized microstructure geometries as well as to carry out simulation to evaluate effective properties and discharge characteristics are highlighted. A brief discussion of the key assumptions and the limitations of such assumptions is also provided.

4.1 Representative microstructure generation

The microstructures used for the evaluation of effective properties were generated using MATLAB's image processing toolbox [50]. As shown in Figure 4.1(a), the positive electrode of a typical Li-ion battery consists of three phases viz. active particles (Ω_{AP}), binder (Ω_B) and electrolyte (Ω_E). Here, only the active particles and electrolyte phases are considered since the aim is to study the effects of active particles distribution on effective properties. An idealized schematic diagram showing the black solid phase active particles and white electrolyte phase is shown in Figure 4.1(b).

A wide range of microstructures across a range of values of effective particle size and volume fraction were generated in order to create a diverse set of compositions of electrodes and analysis was carried out across various electric conductivity ratio values. Figure 4.2 provides a complete picture of the combinations of values of these three

parameters used in this study. For a given volume fraction, the active particles of a particular particle size can be randomly fitted into the microstructure image in a multitude of ways. This in turn may result in the variation of effective properties based on the arrangement of active particles in a certain order. Hence, three different microstructural images were randomly generated to account for the potential variation of effective properties for a given combination of volume fraction and particle size. Figure 4.3(a) provides an illustration of a typical case of three different microstructural geometries that can be generated for a given combination of volume fraction and particle size. It also illustrates a typical active particle geometry with irregular edges. The effective property to be evaluated for each combination of parameters is the average of the individual effective

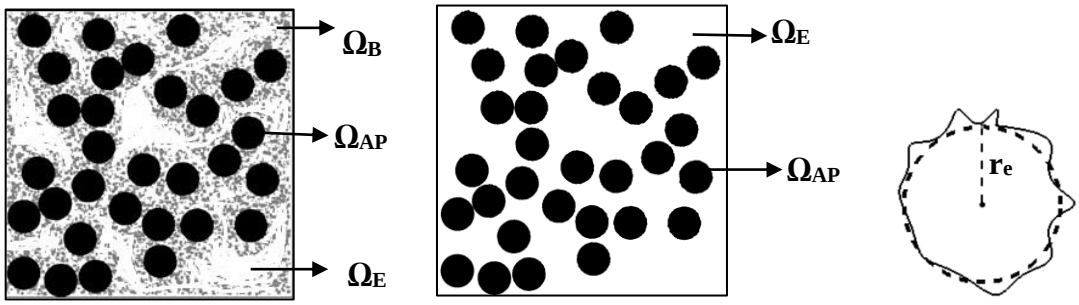

Figure 4.1: (a) A micro-scale schematic diagram showing components of Li-ion cell positive electrode consisting of active particles (Ω_{AP}), binder (Ω_B) and electrolyte (Ω_E) represented by black, gray and white colors, respectively. (b) Schematic of microstructure used for study with black shapes representing active particles (Ω_{AP}) and white space representing electrolyte (Ω_E). (c) Representation of effective radius (r_e) of an arbitrary solid phase particle.

property value of each geometrical arrangement. Depending on the values of the particle size for a given volume fraction, the number of active particles in any microstructure will vary as shown in Figure 4.3(b). The number of particles of the generated microstructures increases from 50 to 19,894 as particle size decreases from 0.4 to 0.001 for this particular case.

All the images generated to represent the idealized microstructures have a resolution of 1000×1000 pixels. The volume fractions of the active particles in the generated images were kept to within 0.05% of the desired value in all the cases. The following sections provide a brief description of the key parameters used for microstructure generation.

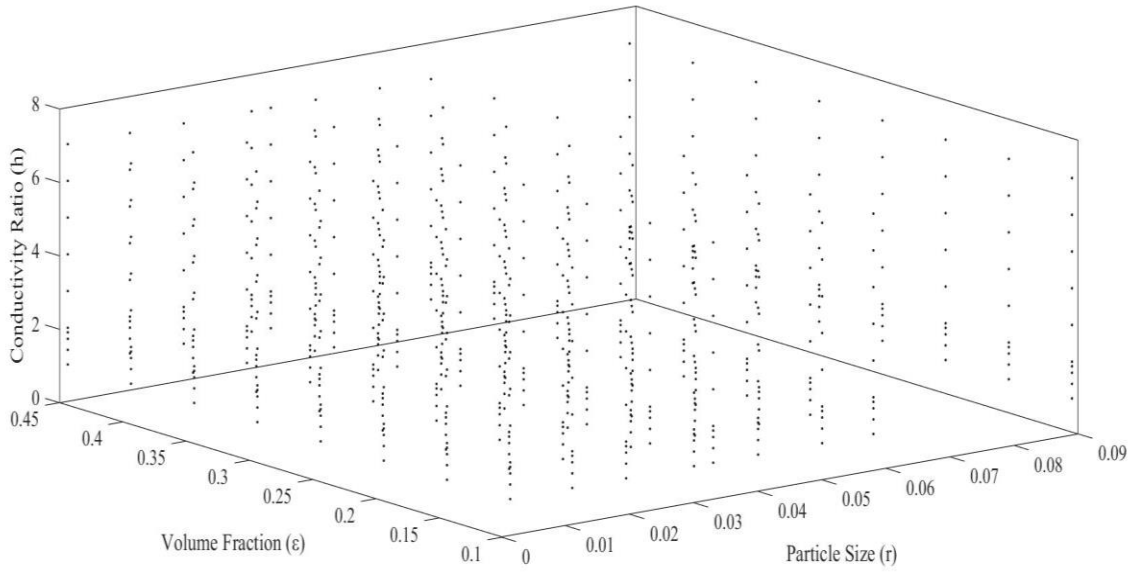

Figure 4.2: Range of values used for study. The values of conductivity ratio (h) are represented in Log_{10} scale. A total of 720 distinct combinations of h, r and ε were used for the study and 3 randomly generated microstructures were used for each combination to evaluate the averaged effective conductivity.

4.1.1 Particle Size

The size of the active particles in any given microstructure is defined using the particle size parameter. It is denoted by r and is defined as the distance from the center of the solid phase active particle to its circumference. This parameter is a dimensionless domain- normalized parameter. From the definition, the particle size of a circular particle is simply the radius divided by the domain width. For any given geometry including the irregular circle shown

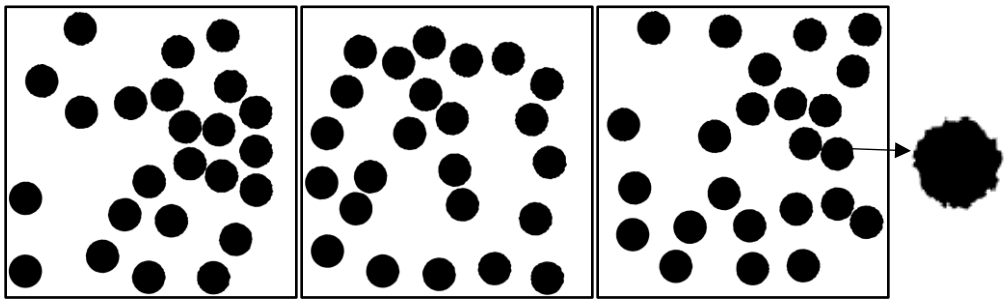

(a)

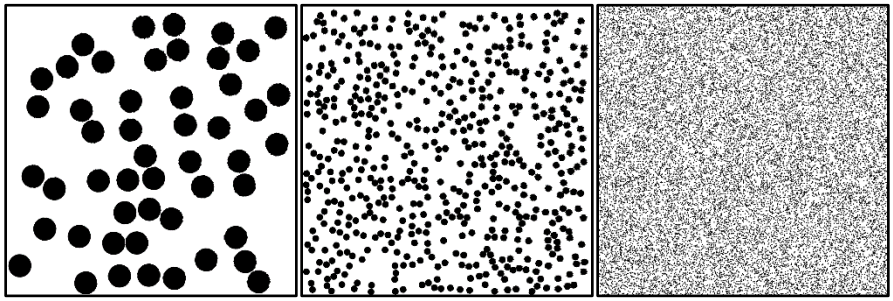

(b)

Figure 4.3: Microstructures generated for study. (a) Three iterations for the same particle size of 0.06 and volume fraction of 0.25 with magnified view of one solid phase particle with irregular edges. (b) Different microstructures for same volume fraction but different radii of approximately 0.04 (N=50), 0.011 (N=553) and 0.001 (N=19,894) respectively from left to right.

in Figure 4.1(c), this can be defined in terms of the radius of the circle of the same area as the actual particle given by $A_{\Omega_{AP}}$. This relationship is given in given in Equation (4.1). For example, if the electrode width is 100 μm then a value of r = 0.05 represents the actual particle size of r = 0.0005 μm.

$$r = r_e = (A_{\Omega_{AP}}/\pi)^{1/2} \tag{4.1}$$

4.1.2 Volume Fraction

The volume fraction for a given microstructure is represented as the fraction of area occupied by the black solid phase active particles as shown by Equation (4.2). For the cases in which the dominant phase is the electrolyte phase, the volume fraction of electrolyte is used which is given by Equation (4.3).

$$\varepsilon_{AP} = \sum A_{\Omega_{AP}} / \sum A_{\Omega} \tag{4.2}$$

$$\varepsilon_E = 1 - \varepsilon_{AP} \tag{4.3}$$

4.1.3 Conductivity Ratio

Conductivity ratio, h, defines the ratio of actual conductivity of the solid phase active particles to that of the electrolyte phase:

$$h = \sigma_{AP}/\sigma_E \, . \tag{4.4}$$

4.2 Simulation using COMSOL

COMSOL Multiphysics® modeling software was used to evaluate the effective properties as well as to illustrate discharge characteristics of an idealized Li-ion cell [48]. In both cases, MUMPS direct solver was used for numerical simulation. In the following sections, a brief discussion on steps used for simulation using COMSOL for the study is presented.

4.2.1 Evaluation of Effective Properties

Desired effective property tensor for the randomly generated two-phase microstructures were evaluated by solving Equation (3.1) in COMSOL using MUMPS solver. This equation was subjected to periodic boundary conditions to comply with assumption (a) of Section 3.1. Mesh generation for the simple square geometry used in this study was created using COMSOL's built-in features. Very fine triangular mesh was used for all simulations based on the results of mesh dependency tests. Results of one of these tests is plotted in Figure 4.4. The final refined mesh chosen for study consists of about 0.32 million triangular elements.

As highlighted in Section 3.1, the information on the geometry is directly obtained from the generated images when they are imported in COMSOL as analytical functions. Presence of the phase associated with active particles is identified by detecting the presence of the black-colored shapes in each image. Chapter 2 contains information on the typical values of intrinsic properties of electrode constituents which are used for the evaluation of effective properties in this study.

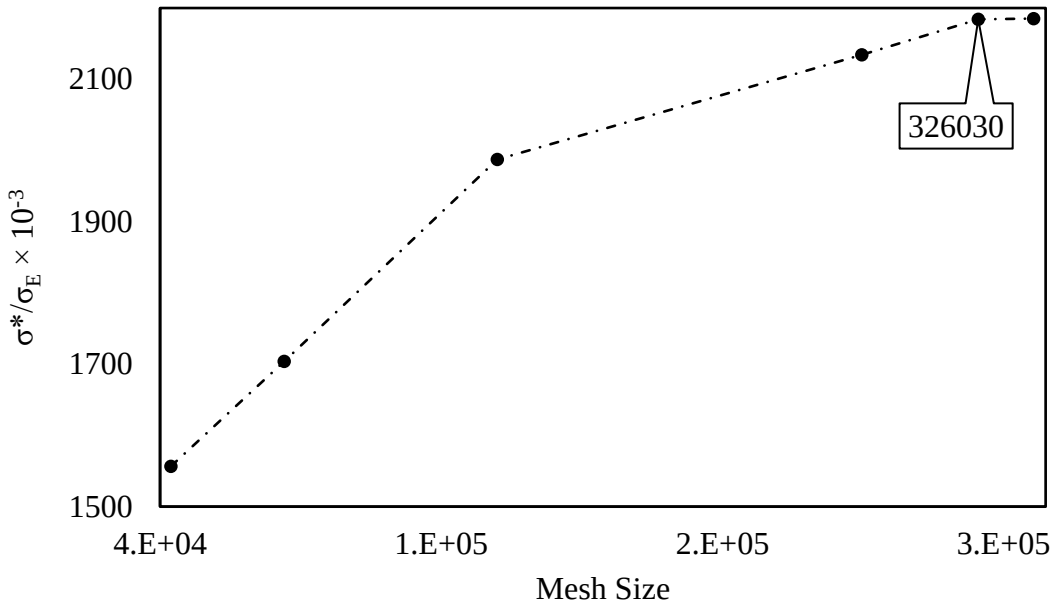

Figure 4.4: Normalized effective conductivity value variation with change in mesh sizes for h = 10^7, r = 0.0073 and ε_{AP} = 0.4. The final mesh consisted of 3,26,030 elements.

4.2.2 Study of Discharge Characteristics

In order to illustrate the effects of consideration of microstructure information on the discharge characteristics of an idealized Li-ion cell, simulation and analysis based on P2D model, described in Chapter 3, was carried out.

All simulations for the evaluation of the discharge characteristics were carried out in COMSOL using its Electrochemistry module [48]. MUMPS solver available in COMSOL was used for all computations. Figure 4.5 represents the schematic diagram of the Li-ion cell used for analysis based on the model is used by Doyle et. al. [25]

Figure 4.5 shows a schematic diagram of a typical Li-ion cell consisting of three main components based on this model. The negative and positive electrodes of lengths L_N and

L_P respectively are kept apart by using separator of length L_S. Both electrodes consist of two phases namely, the electrolyte (white part) and the active particles (dark part). Further, active materials represent carbon and lithium manganese dioxide particles for positive and negative electrodes respectively. The current collectors for the negative and positive electrodes are represented by – and + respectively. Simulation was carried out to evaluate the discharge characteristics at different discharge rates. A more detailed description on the parameters used for simulation is provided in Section 5.5.

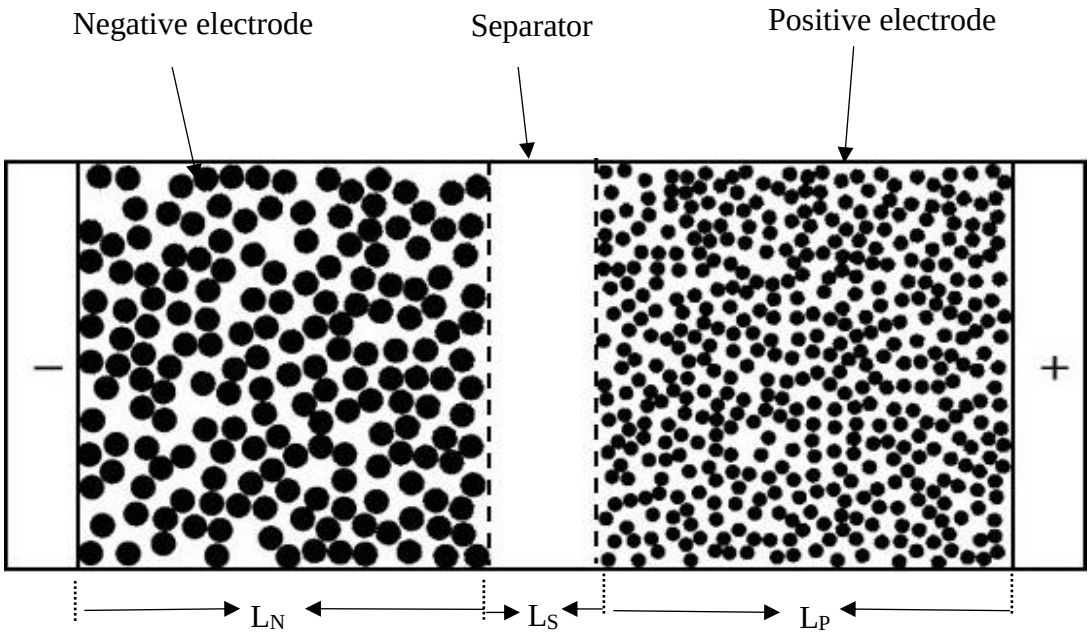

Figure 4.5: Schematic diagram of Li-ion cell consisting of the positive electrode, separator and the negative electrode.

4.3 Assumptions and Limitations

A brief discussion on the assumptions used in this study and the limitations of the study as a consequence of those assumptions is highlighted in this section.

In this study, only two-dimensional (2D) microstructures have been considered to represent the Li-ion battery electrodes. In contrast to the three-dimensional (3D) microstructures, the transport of lithium ions in a 2D microstructure is limited by a parameter called percolation threshold [38]. Above this threshold, the probability of formation of chains and clusters is increased which can act as obstacles to the transport of Li-ions modifying the effective properties. However, this limitation is not as pronounced in 3D microstructures as the Li-ions can navigate the obstacle created by particle clustering using the third spatial direction [38]. Since in this study, particle clustering is not considered and transport is limited to a single plane, the results obtained are only valid below this percolation threshold.

An idealized Li-ion battery positive electrode consists of three phases. But in this study, only the solid phase and electrolyte phase are considered as the significant portion of the research work is focused on highlighting the effect of active phase particle size on the effective properties. As discussed in the literature review section, the Li-ion battery research community is moving towards the development of additive-free cathodes. This research is intended to contribute towards the design of additive-free cathodes and hence excludes the additive (binder/carbon black) phase.

Finally, all the calculations used for the evaluation of effective electrical conductivity and formulation are carried out by considering only the single-particle size distribution. However, an actual battery microstructure cannot be assumed to contain uniformly sized particles. Discussion on the limitation of the use of single-particle size distribution is provided in Chapter 2 and presented further in Section 5.3.

Chapter 5

RESULTS AND ANALYSIS

This chapter contains the results of simulation for the evaluation of effective properties based on the mathematical homogenization method and discharge characteristics of an ideal lithium ion-cell based on the P2D model using the calculated effective properties. A detailed description of the results of the effective electric conductivity evaluation of the Li-ion positive electrode is provided. Results of the evaluation of other effective properties viz. effective diffusivity and effective ionic conductivity are also included.

This chapter is divided into two parts. PART I provides the results and analysis related to the evaluation of effective properties and PART II includes the results and analysis for the evaluation of discharge characteristics based on the calculated effective properties.

PART I: Evaluation of Effective Properties

This part of the Results and Analysis section includes the results and discussion for the evaluation of the effective properties of the positive electrodes based on the mathematical homogenization method. A brief discussion on tortuosity and the results on the comparison with Bruggeman's formulation and effective bounds is also provided. An algebraic formulation is provided in order to demonstrate the effectiveness of the mathematical homogenization approach in the development of empirical formula for the direct evaluation of the effective properties. Discussions on the accuracy and limitations of this formulation are also included in this chapter.

5.1 Evaluation of Effective Electrical Conductivity

The randomly generated representative microstructure images described in Chapter 4 were numerically solved to evaluate the effective values as discussed in Chapter 3. A discussion on the actual properties of each individual phase of a typical Li-ion positive electrode is provided in the Chapter 2. The range of values used for the evaluation of the effective electrical conductivity is provided in Chapter 4.

All simulations for the evaluation of the effective properties were carried out assuming a horizontal (x-) direction transport. Three different instances of the same microstructure geometry were simulated to obtain three estimates of the effective electrical conductivity. As discussed earlier, this was done to account for the potential variation in the effective

properties with the arrangement of solid-phase microstructures in each randomly generated image at given particle size and volume fraction. The three estimates were averaged to obtain a mean effective conductivity value (σ^*). For simplicity, this value is simply referred to as electric conductivity throughout this section.

5.1.1 Effect of Particle Size

Figures 5.1 and 5.2 show the variation of effective electrical conductivity with the change in the size of solid phase particles for specified values of conductivity ratio and volume fraction. The error bars shown in Figures 5.1 and 5.2 represent the variation in the values of σ^* as a result of averaging of three different values from the three respective random microstructure topologies for a particular case. As seen in these figures, for any given microstructure arrangement, the variations in the calculated effective conductivity values between the three different microstructure arrangements for a specified ε_{AP} and r is very small. Further, this difference decreases continuously as the size of the active phase particles increases. This is because the number of possible arrangements of the active phase particles throughout the microstructure image decreases.

For a given volume fraction, conductivity increases when the particle size of the solid phase particles decreases. This inverse relationship can be explained as follows: conductivity is directly related to the number of pathways that exist for the transport of electrons along the x-direction. Although the solid phase particles occupy the same total space inside the microstructure geometry, when the size of the particles is small, there are

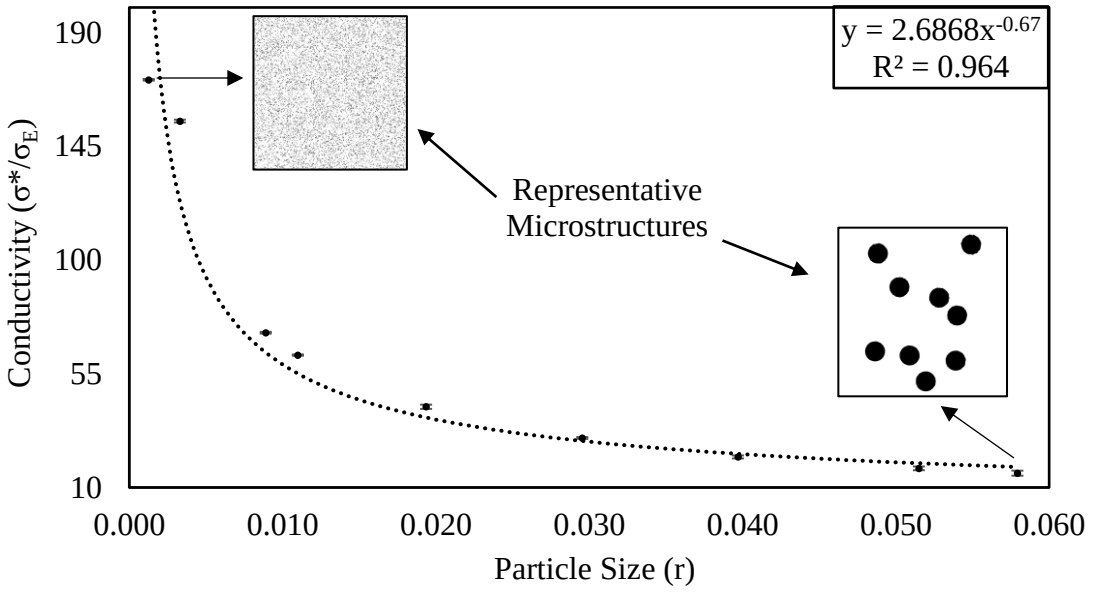

(a)

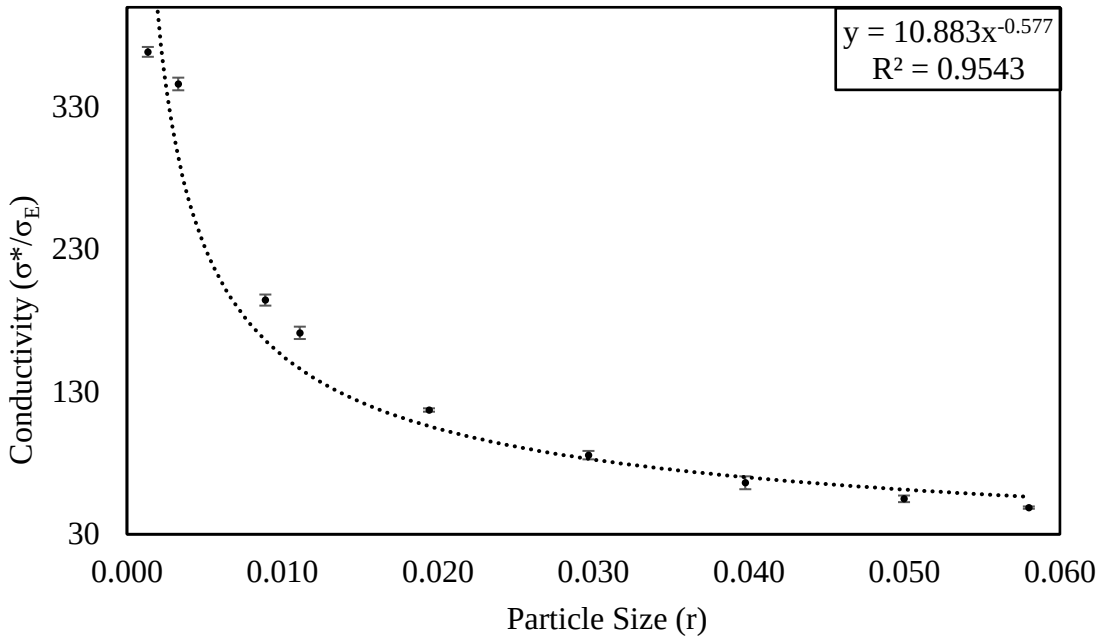

(b)

Figure 5.1: Variation of normalized effective conductivity values with respect to particle size when h=1000 and (a) ε_{AP} = 0.2 (b) ε_{AP} =0.4. The dotted lines indicate the trendline. The two images in (a) are the microstructures associated with given conductivity values.

larger number of active particles available in the domain. This results in an exponential increase in the number of conductive pathways which in turn increases conductivity. For example, in the case of the microstructure geometry images shown in Figure 4.3(b), there are over 19000 particles in the domain with a particle size of 0.001, whereas there are only 50 particles when the particle size is 0.04.

Table 5.1 summarizes the results of evaluation of normalized effective electrical conductivity values for one combination of h and ε_{AP}. In this case, a decrease in particle size from r = 0.05 to r = 0.0013 leads to an increase in the effective electrical conductivity of more than 667%. However, this incredible difference in the values of conductivity cannot be captured by Bruggeman's relationship as it does not consider the effect of the microstructure and only depends on the volume fraction. Based on Bruggeman's formula, as shown for Case C of Table 5.1, the value of effective conductivity is the same for both values of r. For larger particle size (r=0.05), it significantly over-predicts the effective conductivity value whereas it under-predicts the effective value for a smaller particle size (r=0.0013). This highlights the limitation of Bruggeman's formula based on its inability to incorporate the microstructure geometric information.

As shown in Figures 5.1 and 5.2, the relationship between particle size and the normalized effective electrical conductivity of microstructures is well-correlated by the power law. In fact, this relationship is observed for all combinations of h, ε_{AP} and r. In the case of Figure 5.2 (a), the active phase occupies 45% of the microstructure domain and the conductivity ratio, h is 50. Here, when the particle size, r is about 0.02, conductivity starts

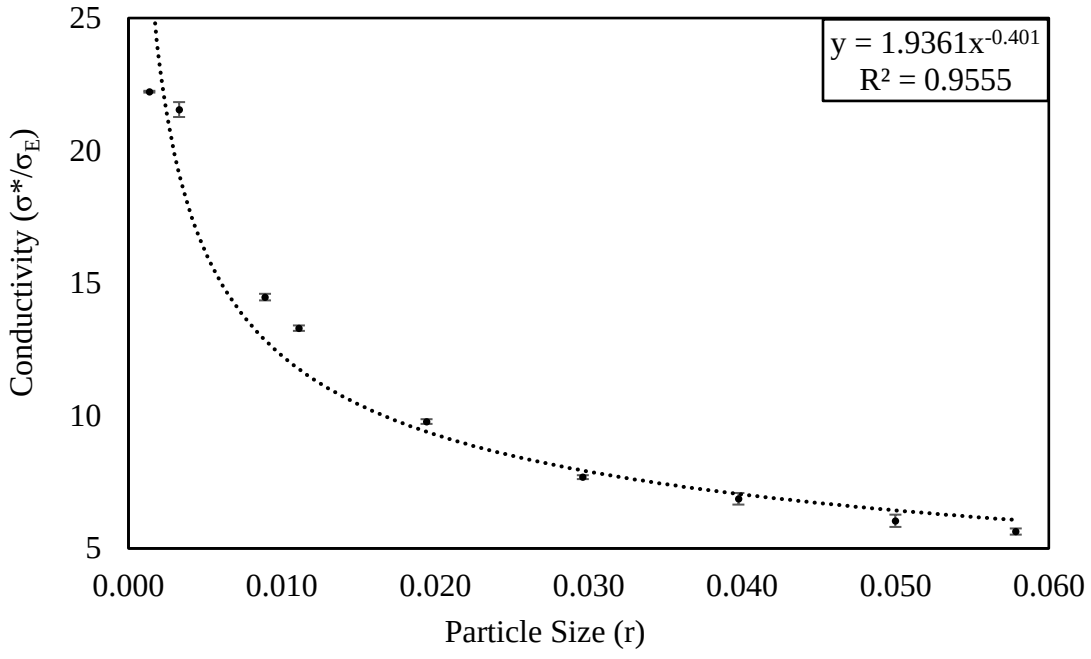

(a)

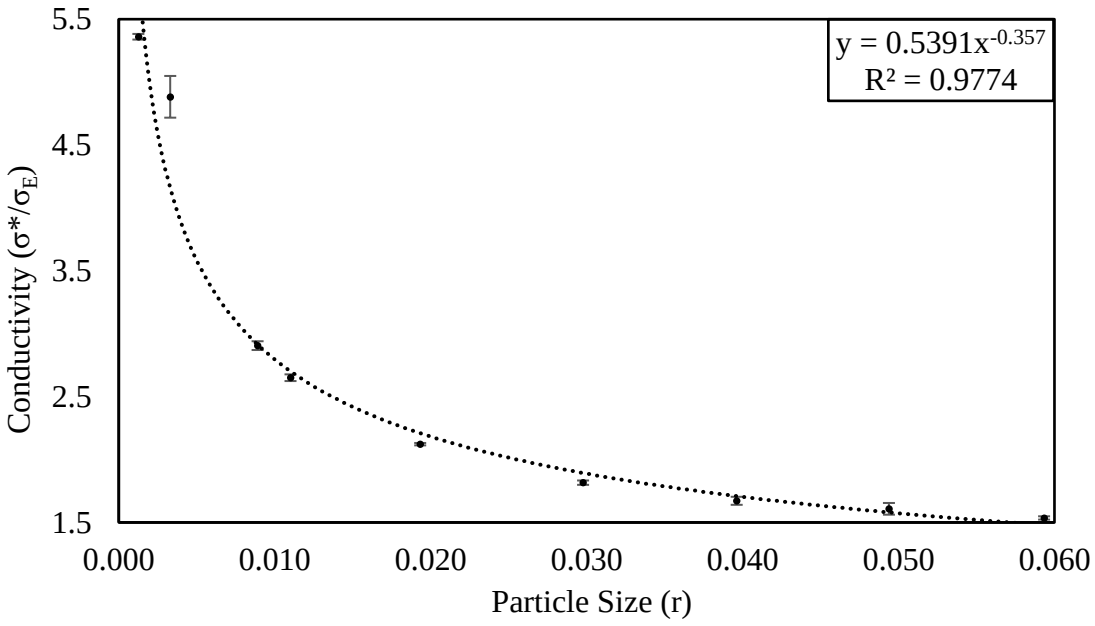

(b)

Figure 5.2: Variation of normalized effective conductivity values with respect to particle size for h=50 and a) ε_{AP} = 0.45 b) ε_{AP} =0.2. The dotted lines indicate trendlines.

to increase more sharply. Again, this relationship between the particle size and conductivity is well correlated by the power-law equation as show in Figures 5.1 and 5.2.

5.1.2 Variation with Volume Fraction

The relationship between volume fraction and effective property values is well established in literature. Figures 5.3 illustrates the variation in the normalized values of σ^* with the change in volume fraction across a range of particle sizes for two different values of h. As expected, the values of normalized conductivity increase with increasing volume fraction of the solid phase. When the amount of the dominating solid phase increases in a microstructure, the dominating property is bound to increase. For instance, as shown in Figure 5.3(a), for a particle size of r=0.001, the normalized conductivity value increases by almost 350% when the volume fraction of the active phase increases from 10% to 45%. A similar trend for the effective conductivity is observed for all other values of h. Again, conductivity is well correlated by the power law equation for all these cases. The dark circles in Figure 5.3 indicate the values of effective conductivity evaluated using the Bruggeman's formula. As evident in this figure, it overpredicts values of effective conductivity for all particles sizes expect when r is significantly small. More generally, for large values of r (big particles), the Bruggeman's formula is expected to overpredict the effective conductivities, whereas it will under predict the same for very small values of r (small particles).

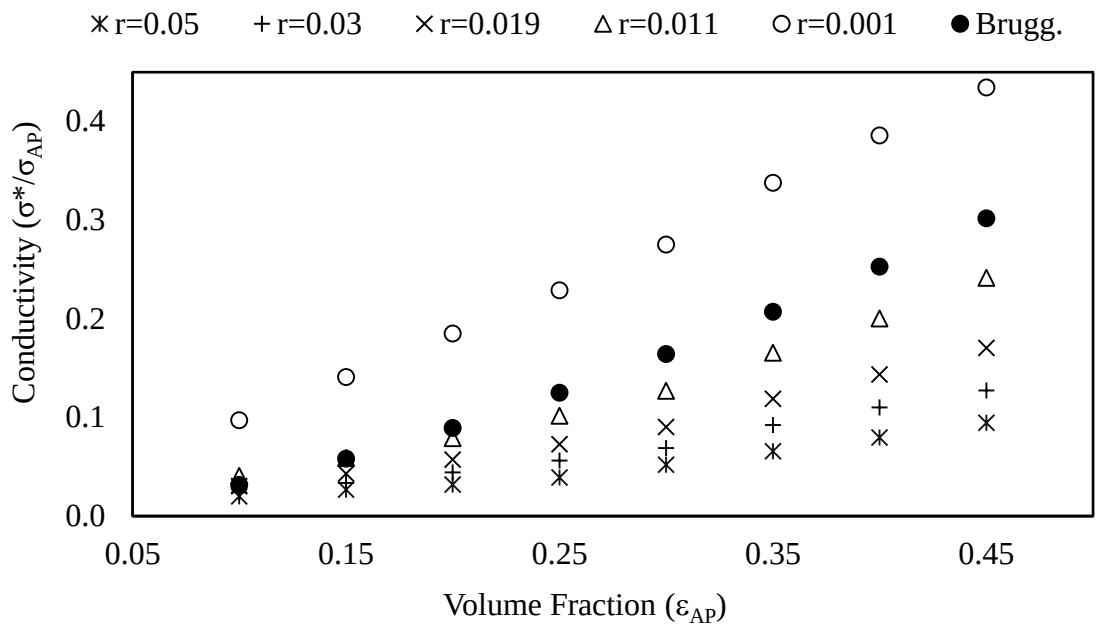

(a)

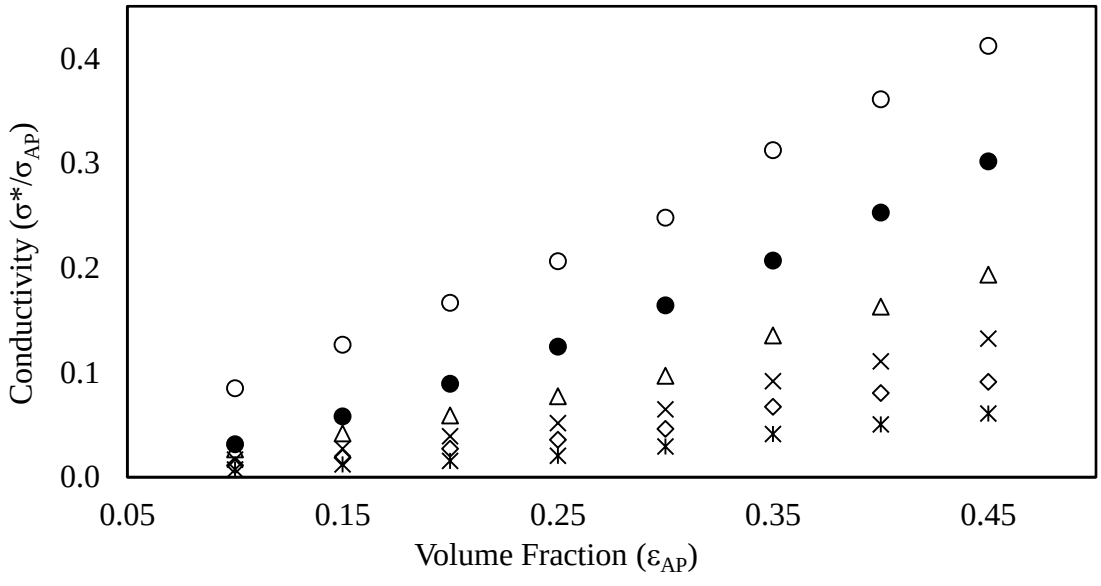

(b)

Figure 5.3: Variation of normalized effective conductivity with volume fraction for different microstructures with different radii when (a) h=10 and (b) $h=10^4$.

Table 5.1: Variation in the value of normalized effective electrical conductivity.

Case	h	ε_{AP}	r	σ^*/σ_{AP}
A	10^6	0.45	0.05	0.0481
B	10^6	0.45	0.0013	0.3586
C	10^6	0.45	(0.05,0.0013)	0.2530

5.1.3 Variation with Conductivity Ratio

The variation of σ*, across a broad range of values of h, as a function of volume fraction with particle size, r = 0.011 is plotted in Figure 5.4. A logarithmic scale is used to fit results of a wide range of values of h. The values of conductivity across a range of volume fractions for a specified value of r increase with an increase in the value of conductivity ratio, h.

This trend is observed for all other values of r that have been considered in the study. As the conductivity ratio value increases, the contribution towards the overall effective conductivity from the dominating phase becomes increasingly significant. This in turn increases the effective value of conductivity as shown by Figure 5.4. For higher values of conductivity ratio, the actual conductivity of the dominating active phase is higher. Hence, the values of effective electrical conductivity increase with the increase in h.

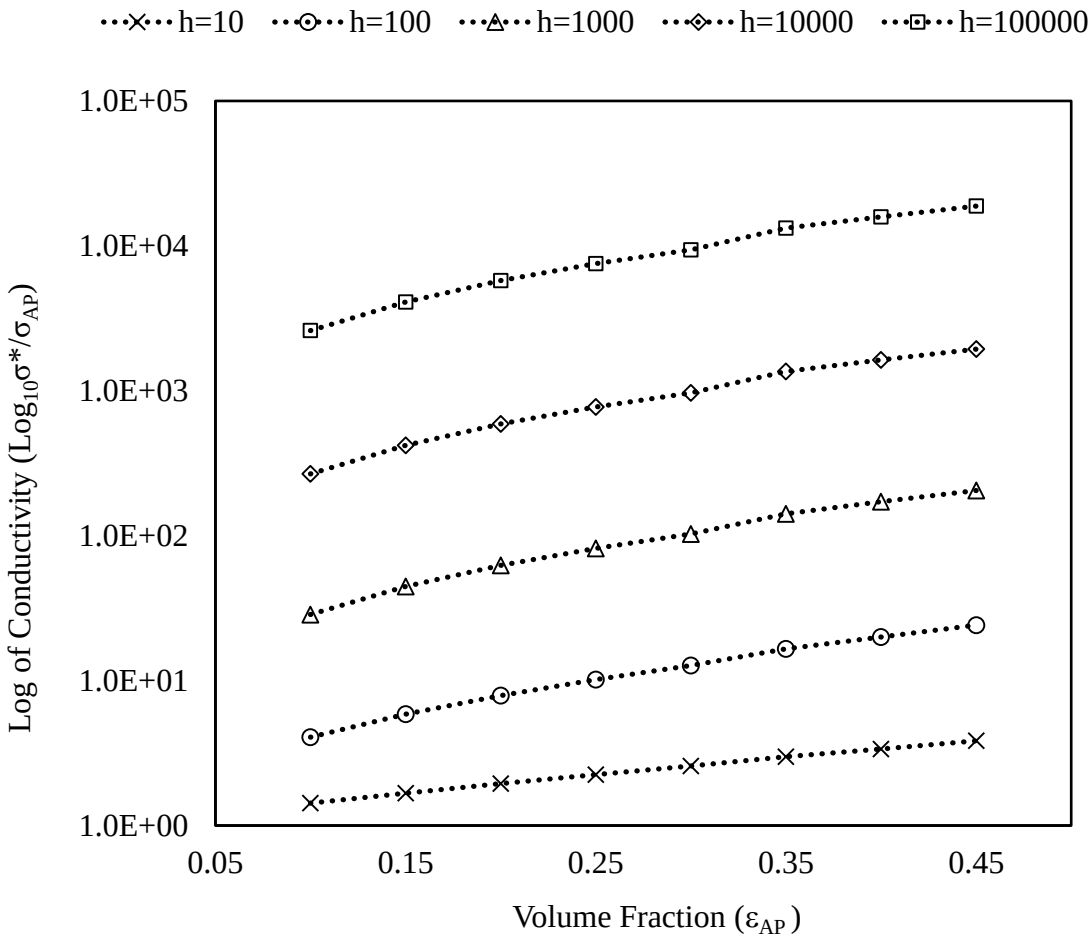

Figure 5.4: Effective Conductivity as a function of volume fraction for different values of conductivity ratios when the particle size, r = 0.011.

5.1.4 Comparison with Effective Bounds and Bruggeman's Formula

In practice, as is the case with composite materials in general, the exact microstructure of the Li-ion battery electrodes cannot be precisely ascertained. Hence, it is easier to obtain the range of possible values of an effective property for given microstructure using partially specified information of microstructure [51]. This method provides a way to

evaluate the optimal bounds of effective values of a property. In essence, effective property bounds of the randomly generated microstructures provide the upper and lower limits of the expected values of the property. In this section, the results obtained using the proposed mathematical homogenization method were compared with these effective bounds as well as Bruggeman's formula for a range of microstructures.

If the microstructure in question can be assumed to be statistically isotropic, the Hashin-Shtrikman (H-S) bounds can be used to obtain tighter upper and lower bounds of effective conductivity values [5]. If the microstructure cannot be assumed to be isotropic, the Weiner bounds can be used , which provide a wider range of optimal values [52]. These Weiner bounds utilize the information on volume fraction and individual conductivities to provide the upper and lower limits of the values of effective properties. For a two-phase microstructure, the Weiner bounds, in terms of the conductivity ratios, are written as [3]:

$$\sigma^*_{\mathrm{L}} = \sigma_{\mathrm{E}} \left(\varepsilon_{AP}/\mathrm{h} + \varepsilon_{\mathrm{E}}\right)^{-1} \tag{5.1}$$

$$\sigma^*_{\mathrm{U}} = \sigma_{\mathrm{E}} \left(\varepsilon_{AP} \times \mathrm{h} + \varepsilon_{\mathrm{E}}\right)^{-1} \tag{5.2}$$

Comparison of the values for effective conductivity obtained from homogenization method with the values of Weiner bounds and Bruggeman's formula is shown in Figures 5.5 and 5.6 for two different values of conductivity ratio, h. As shown in Figure 5.5, as the particle size decreases from a value of r=0.058 to r=0.001, the value of effective conductivity becomes twice as large based as per the mathematical homogenization method. This difference in the values of effective conductivity becomes starker for higher conductivity

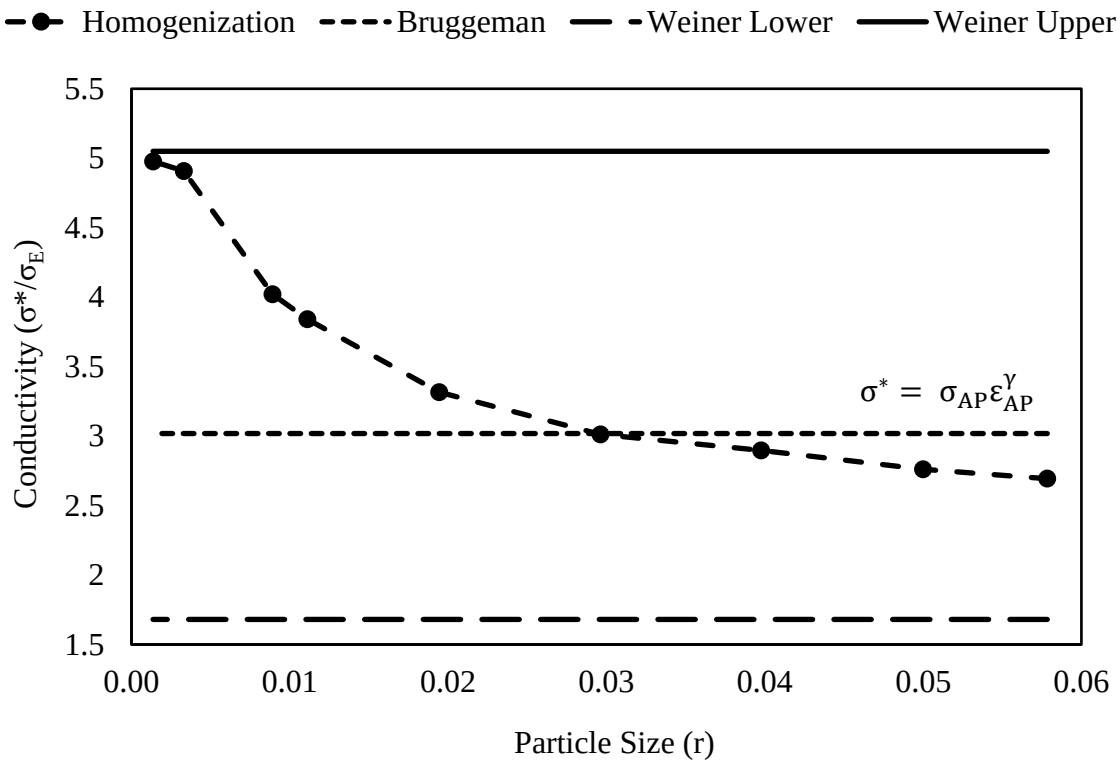

Figure 5.5: Comparison of effective conductivity values from the mathematical homogenization technique with Bruggeman's formula for two different microstructures as a function of the particle size for h = 10 and ε_{AP} = 0.45.

ratio values as seen in Figure 5.6. However, since Weiner bounds and Bruggeman's formula only use the information of volume fraction and individual conductivities, they have a constant value irrespective of the size of the particles. On the other hand, the effective conductivity value obtained from homogenization method is different for different particle sizes. Put differently, the microstructure changes as the particle size varies, and the homogenization method takes this into account while estimating the effective conductivity.

It must be noted that, all these values across the spectrum of particle sizes fall within the rigorous Weiner bounds for all cases considered in this study. As the particle size decreases, the effective conductivity values move closer and closer to the rigorous upper bound. This means that the use of smaller solid phase particles for a given volume fraction leads to more optimal conductivity values. This is expected because with an increased number of smaller particles spread over the domain, the number of conductive pathways available to transport electrons increase significantly.

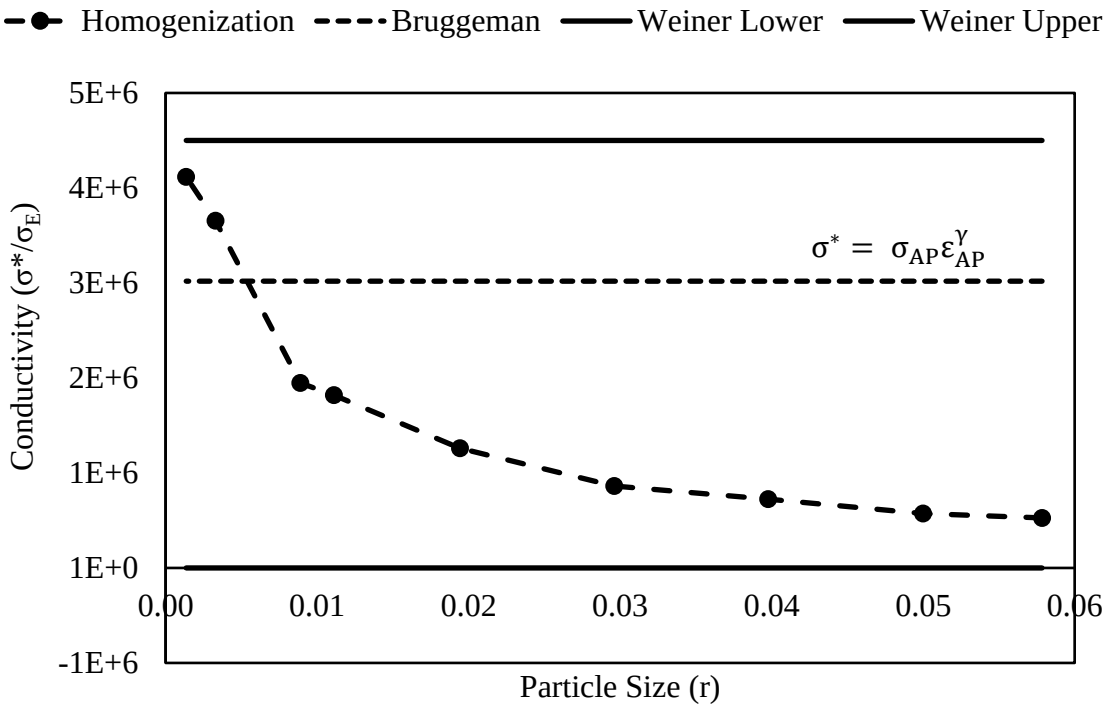

Figure 5.6: Comparison of effective conductivity values from the mathematical homogenization technique with Bruggeman's formula for two different different microstructures as a function of the particle size for h = 10^7 and ε_{AP} = 0.45.

5.2 Algebraic Formulation to Evaluate Effective Conductivity

Results of numerical study in the previous sections indicate that effective conductivity varies with conductivity ratio, particle size and volume fraction of the particles. These relationships are found to follow certain trends across a wide spectrum of values of h, r and ε_{AP}, a few examples of which are given in Figures 5.1, 5.2, 5.3 and 5.4. In this section, based on the trends like these across a wide range of values of h, r and ε_{AP}, an explicit formulation for the evaluation of effective electrical conductivity as a function of conductivity ratio h, particle size r and volume fraction of solid phase ε_{AP} is proposed. This can be written as:

$$\sigma^* = f(h, r, \varepsilon_{AP}). \tag{5.3}$$

Specifically, a few algebraic manipulations of the relationships between σ* and h, r and ε_{AP} leads to the following form:

$$\sigma^*/\sigma_E = A_1(h) \times r^{B_1(h)} \times \varepsilon_{AP}^{A_2(h) r^{B_2(h)}}, \tag{5.4}$$

where A_i and B_i are coefficients that are functions of h.

From the analyses of the results of previous sections, the coefficients A_i and B_i in Equation (5.4) are likely to vary with conductivity ratio. To improve the accuracy of the formula, separate studies were carried out for a range of values of h <= 100 and h > 100. Figures 5.7 and 5.8 show that the variation of the coefficients of the formulation (A_1, A_2, B_1 and B_2) across a range of values of h for h>100 in log scale is in an almost perfect

agreement with the trendline. Based on this, these coefficients in general form can be written as:

$$A_1 = A_{11}.h^{A_{12}} \tag{5.5}$$

$$B_1 = B_{11}.h^{B_{12}} \tag{5.6}$$

$$A_2 = A_{21}.h^{A_{22}} \tag{5.7}$$

$$B_2 = B_{21}.\ln(h) + B_{22} \tag{5.8}$$

Similarly, an analysis was done for h <=100, and revised coefficients in Equations (5.5)-(5.8) were established. The values of the coefficients for the two ranges of h are summarized in Table 5.2. In the ensuing section, a rigorous analysis of the proposed formulation is carried out and the error in calculation for different combinations of values including the ones not directly calculated in this section is analyzed.

Table 5.2: Value of coefficients of the algebraic formula for calculation of effective conductivities.

h	**A_{11}**	**A_{12}**	**B_{11}**	**B_{12}**	**A_{21}**	**A_{22}**	**B_{21}**	**B_{22}**
h<=100	0.7136	0.4076	0.1189	0.3219	0.1676	0.4173	0.0379	0.17198
h>100	0.0503	0.9885	0.4957	0.0014	1.7349	0.0079	0.0013	0.07232

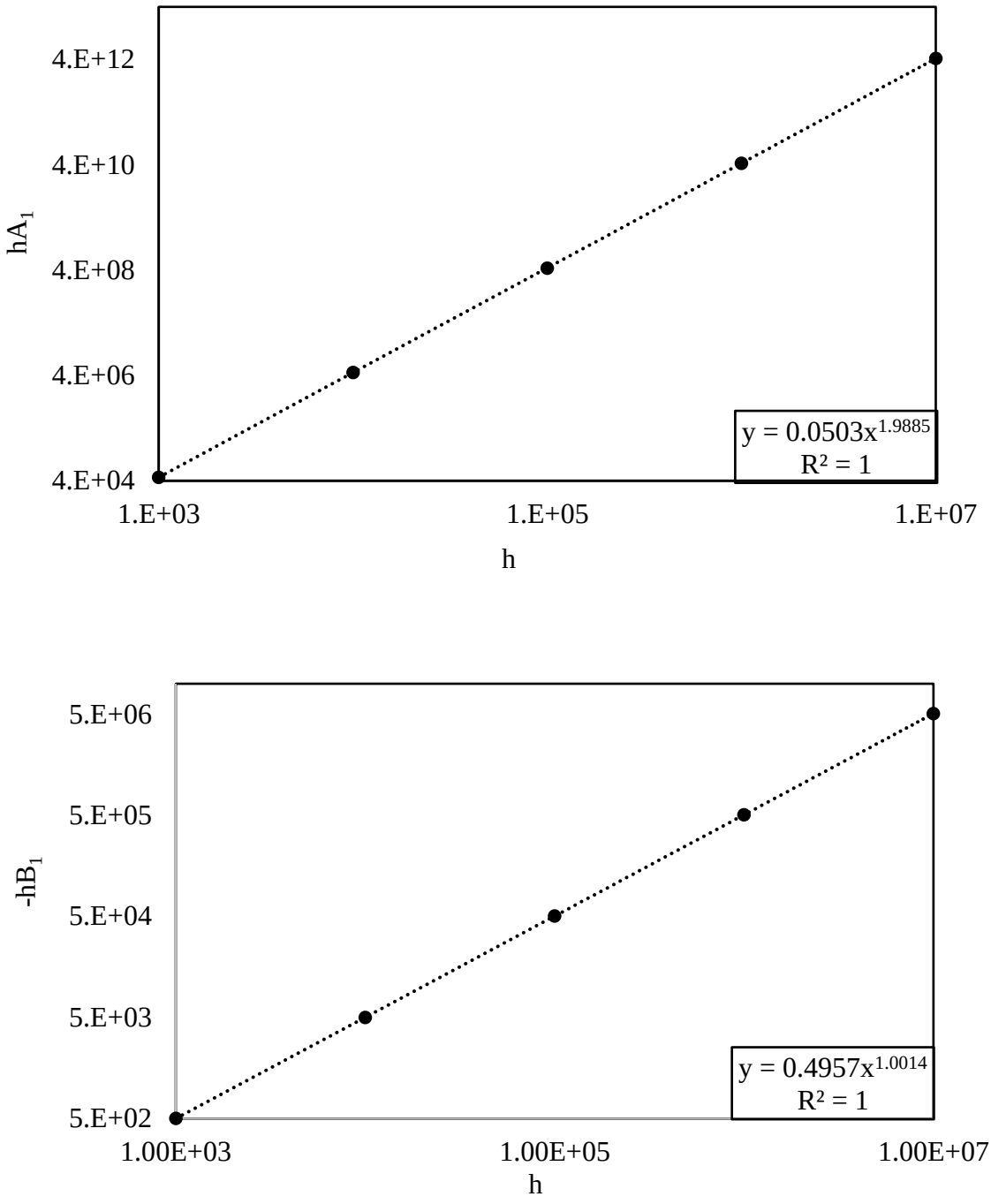

Figure 5.7: Variation of the coefficients of formulation A_1 and B_1 across a range of values of h for h > 100. For clarity of representation, both axes are presented in logarithmic scale and the y-axis values are scaled by h. The dotted lines represent the trendline.

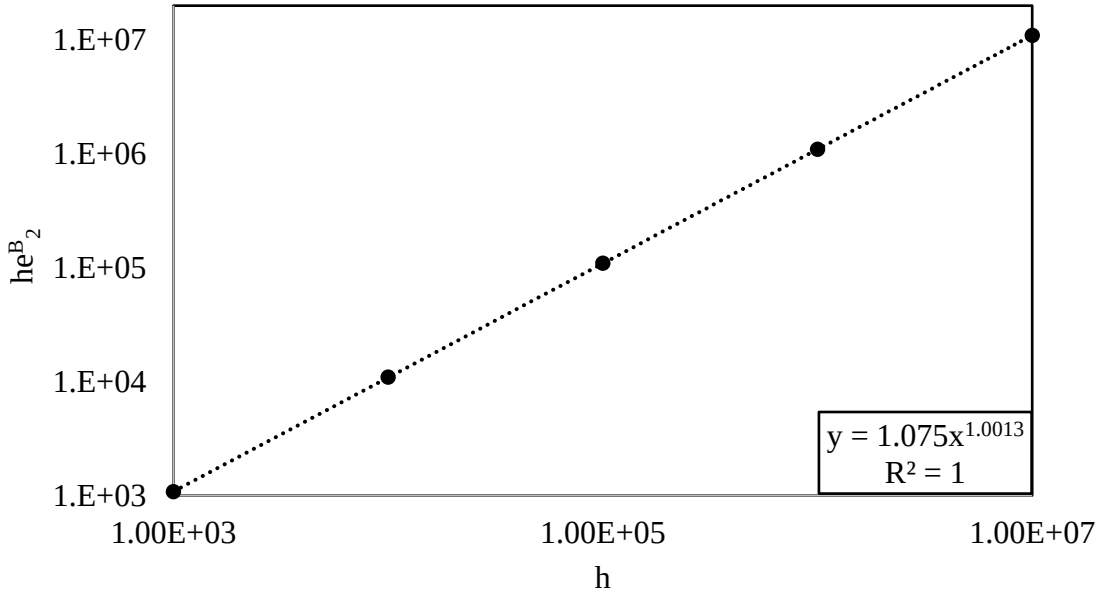

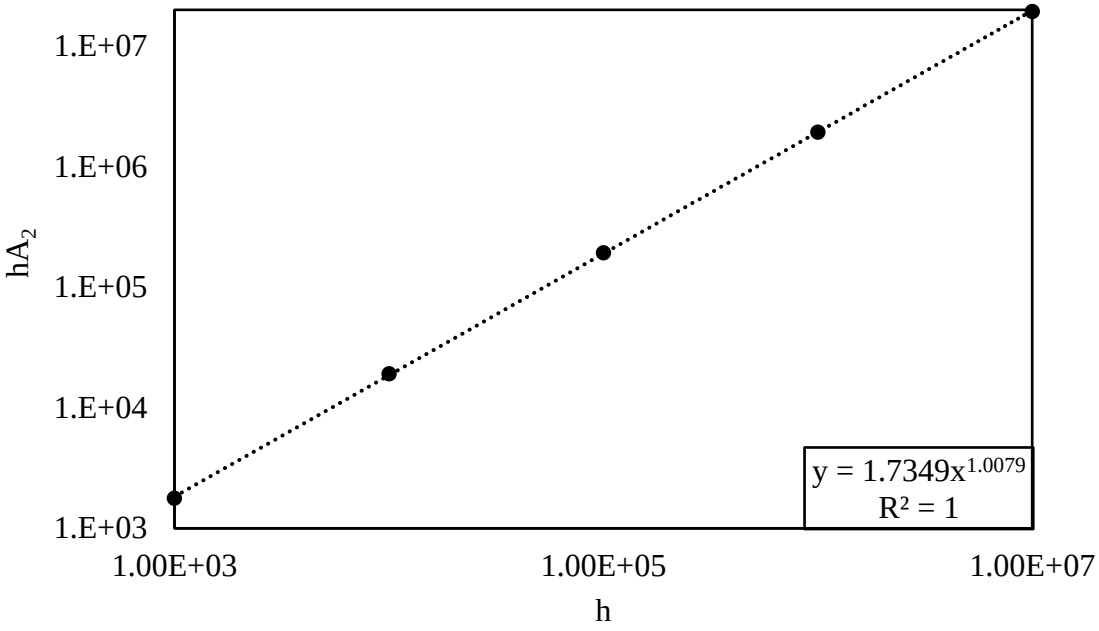

Figure 5.8: Variation of the coefficients of formulation A_2 and B_2 across a range of values of h for h > 100. For clarity of representation, both axes are presented in logarithmic scale and the y-axis values are scaled by h. The dotted lines represent the trendline.

5.2.1 Analysis of Proposed Formulation

In this section, analysis of the formulation proposed in Equation (5.4) is carried out that describes the effective electrical conductivity as a function of particle size, volume fraction and conductivity ratio, thereby adequately taking into account the microstructural information. For this, 100 different combinations of r, h and ε_{AP} were considered for each range of h, i.e., h <= 100 and h > 100. Figure 5.9 shows a comparison of the effective conductivity values from Equation (5.4) and the mathematical homogenization, the latter being assumed as the actual value. The average relative error is approximately 8% for these 200 cases. There are diverse sources of errors, such as the averaging of values, and errors of estimate accumulated because of the use of multiple trendlines for prediction. Additionally, during the stage of microstructure generation, values of the volume fraction are within a 0.05% range of the desired volume fraction, which also contributes to the overall error.

In reality, the shape and size of the microstructure particles aren't properly defined. Homogenization method used in this thesis provides a way to evaluate effective properties by identifying the different phases present in the microstructure. This means that the results based on this method and hence the proposed formulation will not be dependent on the shape of the particles inside the microstructure. To show that Equation (5.4) is valid for solid-phase particles of various shapes, three other theoretical shapes of the active particles were considered. Figure 5.10(a) shows the representative microstructures with these three shapes, namely square, triangle and circle. The particle size for these shapes are defined according to the definition provided in the representative microstructure generation

section. Effective conductivity values were obtained for a range of values of h, r and ε_{AP} from mathematical homogenization technique as well as the formulation proposed in Equation (5.4). A comparison of the results from Equation (5.4) (predicted values) and the homogenization technique (actual values) is presented in Figure 5.10(b). Once again, a strong correlation between the actual and predicted values is observed. The average relative

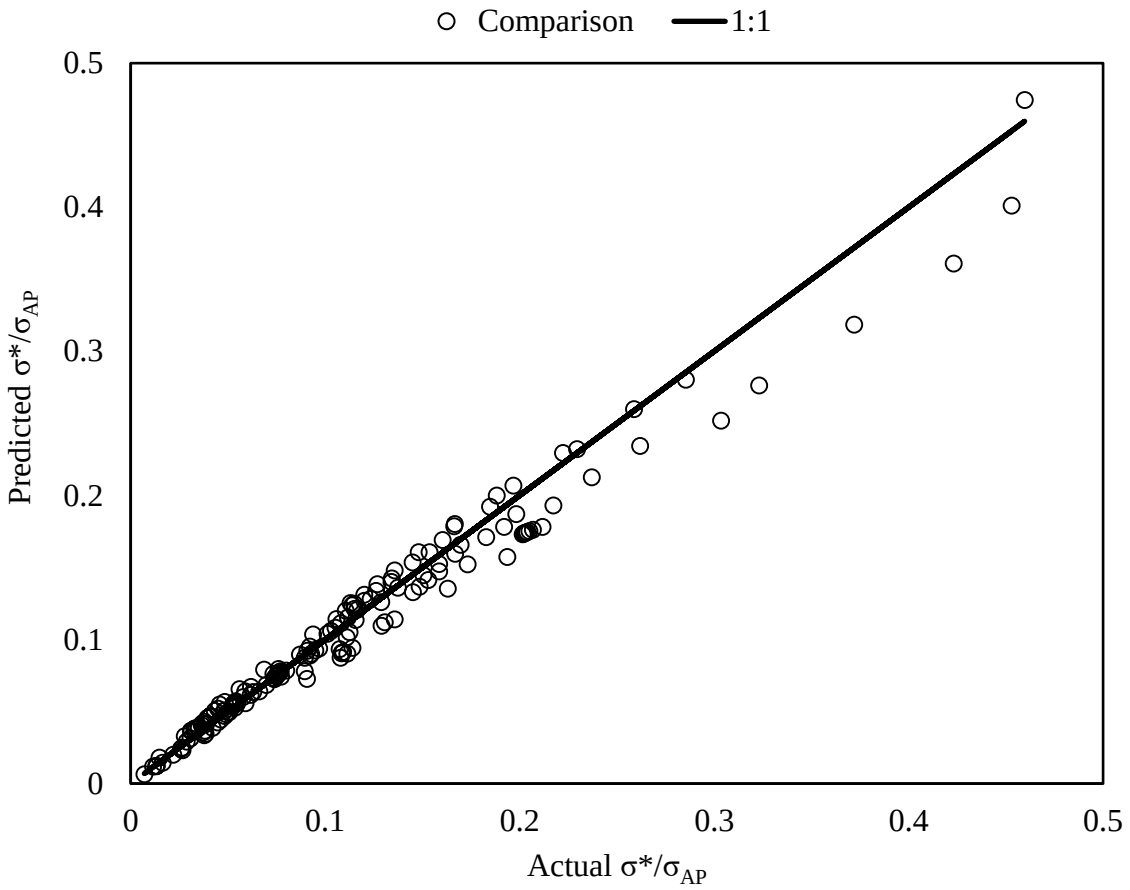

Figure 5.9: Comparison of the explicit formulation predicted values of conductivity normalized by conductivity ratio with the actual values from simulation based on homogenization method across a range of values of h, r and ε_{AP}.

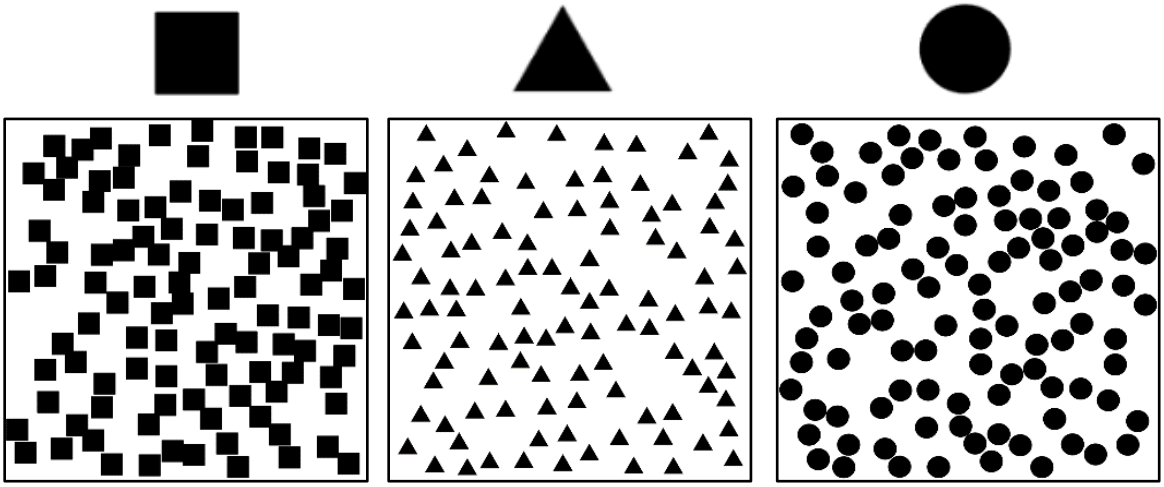

(a)

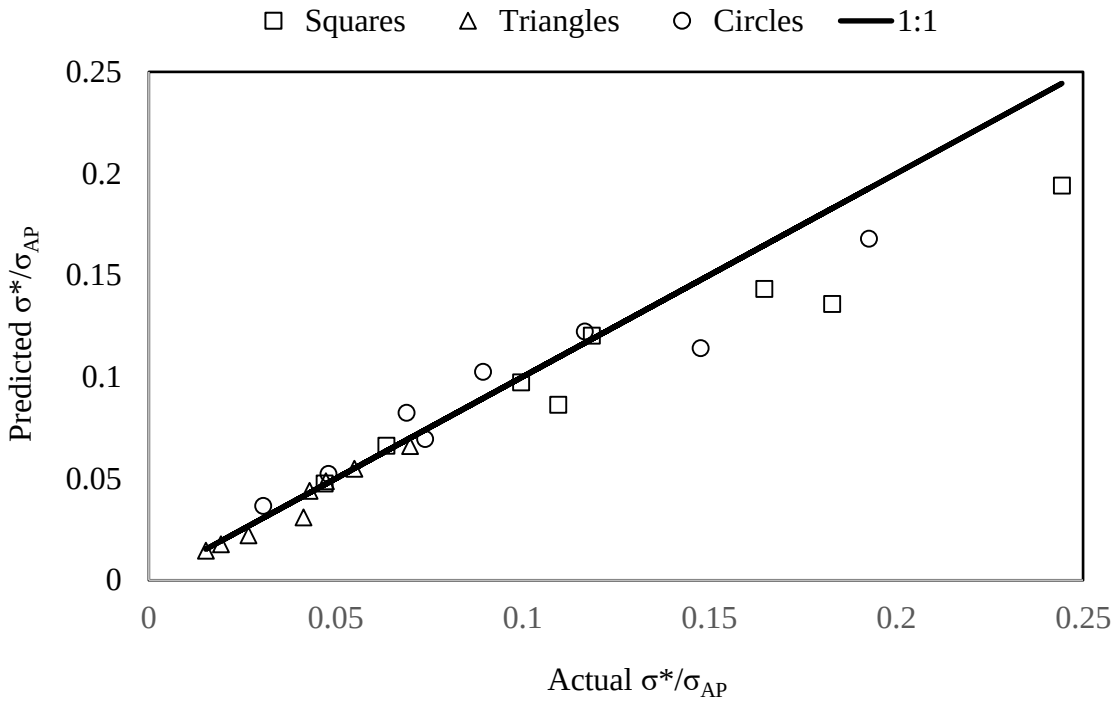

(b)

Figure 5.10: (a) Microstructures of square, triangular and circular shapes from left to right with magnified views of shapes for different values of r and ε_{AP}. (b) Comparison between predicted values of normalized conductivity using proposed formulation with actual values based on homogenization method for different shapes of solid-phase particles.

error for the square, triangular and circular shapes are approximately 11%, 8% and 14% respectively.

5.2.2 Discussion

In conclusion, based on the relationship of σ^* with h, r and ε_{AP}, an explicit formulation has been provided. The main aim of this analysis is to provide a formalism to easily and explicitly evaluate the effective properties of a typical Li-ion battery positive electrode. This is based on a highly simplified model and the resulting equation should only be used by considering all the limitations which provided in section 4.3. However, there is a potential for the extension of this formulation to incorporate multi-modal particle size distributions and all three phases of a typical electrode microstructure (i.e. binders with C-additives, active particles and electrolyte) for a 2D or 3D model. This would help provide a more accurate value of the effective conductivity for the electrodes. Finally, similar formulation can also be derived based on the calculation of other effective properties including the ionic conductivity and diffusivity.

5.3 Effect of Particle Size Distribution on Conductivity

As discussed earlier, actual microstructures of the Li-ion battery positive electrodes may not contain active particles of the same size. In reality, particles of different sizes are distributed throughout the domain. However, modeling of the electrodes by considering all of the particle sizes is computationally infeasible as there can be a tremendous difference in the combinations of particles of different sizes based on the method of fabrication [53]. The often used P2D model utilizes only a single-particle size distribution model [25]. Darling et al. [54] provided an extended version of the P2D model by using two characteristic particle sizes. Recently, Taleghani et al. [37] extended this model further by using a 3-particle model. They provided a comparative study of discharge characteristics of Li-ion battery based on the consideration of a single-particle, bi-modal and 3-particle size distribution in positive electrodes using the P2D model.

In this section, effective electrical conductivity based on a bi-modal particle size distribution are calculated and compared with the results based on the mono-modal size distribution used in earlier sections. Figure 5.11 shows two microstructures of same average volume fraction and particle size generated using single-particle and bi-modal particle size distributions. In this case, there are 295 particles for a single-particle distribution and 149 particles each (i.e. total 298) of two different sizes for the bi-modal particle size distribution. Number of particles for the bi-modal distribution depends on two main parameters including the ratio of particle sizes of the two representative particle types and individual volume fractions of each particle type. For comparison of the mono- and bi-

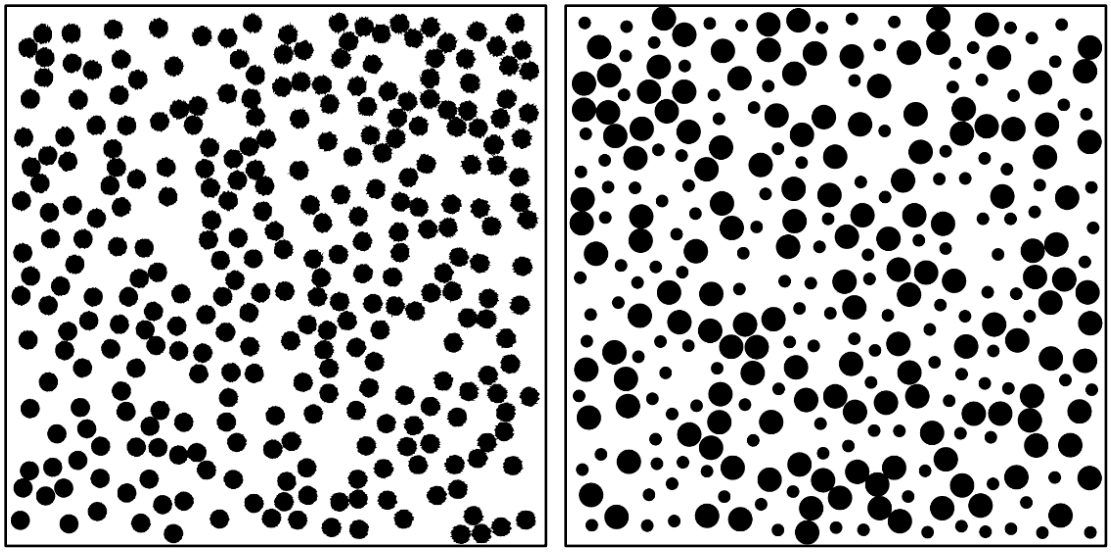

Figure 5.11: Microstructure images representing two distinct types of particle size distribution viz. mono-modal (N=295) and bi-modal when $\varepsilon_{AP} = 0.3$ and $r \approx 0.0165$. For bi-modal case, $\varepsilon_1:\varepsilon_m = 0.2$, r_2: $r_1 = 2$ and N=149 each for both small and big particles.

modal particle size distributions, the average of two different particle sizes in bi-modal is made to be equal to the particle size of the mono-modal case. i.e.

$$r = (r_S + r_L)/2 \,. \tag{5.9}$$

Similarly, the average volume fraction of the active phase in the bi-modal distribution is equal to the volume fraction of the solid phase of the single-particle distribution. The bi-modal particle based microstructures were generated by assuming that the mass and specific surface area of the active particles in bi-modal distribution to be equal to the mono-modal case [37,54]. Based on these assumptions, volume fraction for the bi-modal case was evaluated by using equations (5.10 and 5.11) [54]:

$$\frac{\varepsilon_S}{\varepsilon_{AP}} = \frac{r_L/r - 1}{r_L/r_S - 1}, \tag{5.10}$$

with

$$\frac{\varepsilon_S}{\varepsilon_{AP}} + \frac{\varepsilon_L}{\varepsilon_{AP}} = 1, \tag{5.11}$$

where, the subscripts L and S represent large and small particles in bi-modal distribution and r and ε_{AP} represent the particle size and volume fraction for the mono-modal distribution consistent with the description in previous sections. A value of $h=10^7$ is used for all the cases in this section.

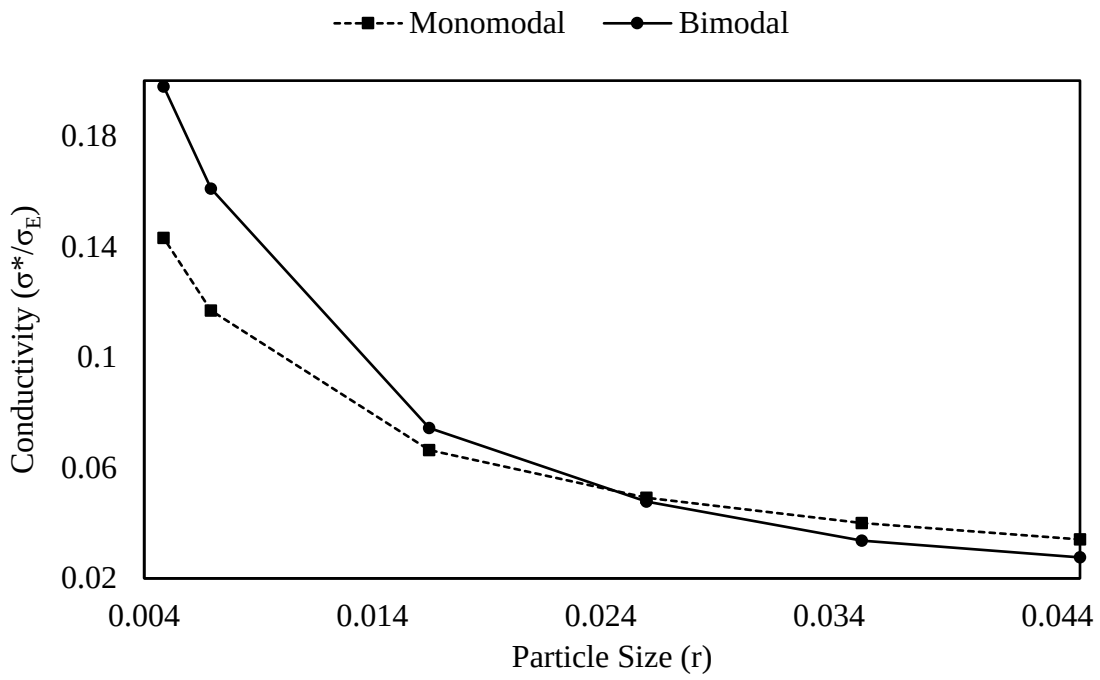

Figure 5.12: Comparison of normalized effective electrical conductivity between mono-modal and bi-modal distribution microstructures when $\varepsilon_{AP} = 0.3$ with $\varepsilon_S:\varepsilon_{AP} = 0.2$ and $r_L: r_S = 2$ for bi-modal distribution.

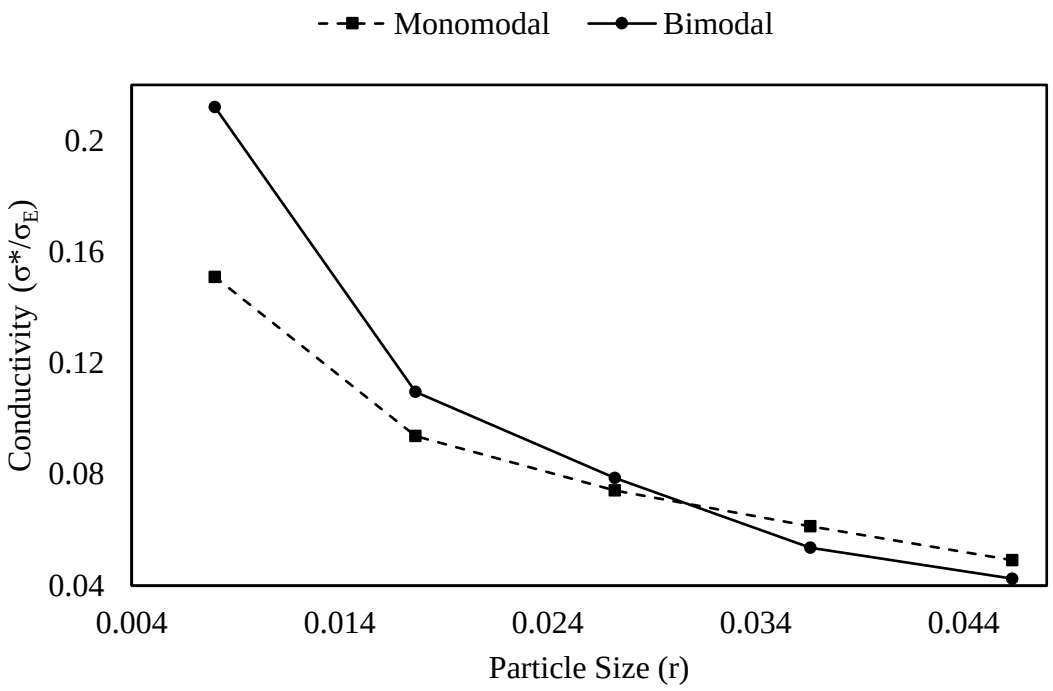

Figure 5.13: Comparison of normalized effective electrical conductivity between mono-modal and bi-modal distribution microstructures with $\varepsilon_{AP} = 0.4$ with $\varepsilon_S:\varepsilon_{AP} = 0.2$ and $r_L: r_S = 1.6$ for bi-modal distribution.

Figures 5.12 and 5.13 provide results of comparison of effective electric conductivity values considering mono-modal and bi-modal distributions. In Figure 5.12, variation of conductivity across a range of values of average particle size for an active particle volume fraction, $\varepsilon_{AP} = 0.3$ with $\varepsilon_S:\varepsilon_{AP} = 0.2$ and ratio of particle sizes, $r_L: r_S = 2$ is provided. For larger particle sizes, the difference between the conductivity values obtained using mono- and bi-modal distributions is not very significant. In fact, a mono-modal particle size distribution seems to provide a slightly better effective conductivity for these large particle size cases. However, as the average particle size decreases, the effective conductivity values with the bi-modal distribution increases at a higher rate than with the mono-modal

distribution. For an average particle size, r=0.00485, the effective conductivity for bi-modal distribution is about 38% greater than that for mono-modal distribution.

A similar trend is observed in the case of Figure 5.13 when $\varepsilon_{AP} = 0.4$, $\varepsilon_S:\varepsilon_{AP} = 0.2$ and $r_L: r_S = 1.6$. Both particle size distributions have similar values up until r=0.027. For particle sizes greater than this value, however, a significant difference in effective conductivities is observed. At the average particle size of r=0.008, effective conductivity for the bi-modal distribution is about 40% greater than that for the mono-modal distribution. This is because at smaller particle sizes, the number of particles for bi-modal distribution are significantly greater than that for the mono-modal case. This means, for bi-modal distribution, there are more conductive pathways which results in an increased effective conductivity. Similar trends are observed for all other cases with different combinations of particle sizes and volume fractions. This highlights the limitation of assuming only one particle size as is done in most literature using P2D model.

5.4 Evaluation of Other Effective Properties

As discussed earlier, the homogenization method described in this study can be employed to evaluate other effective properties of Li-ion battery positive electrode including ionic conductivity and diffusivity. In this section, analysis of a few results of the evaluation of effective ionic conductivity and diffusivity are provided.

5.4.1 Evaluation of Effective Diffusion Coefficient

The value of diffusion coefficient of the Li+ ions in electrolyte is greater than in the solid-phase (see Chapter 2). Hence, electrolyte phase is the dominating phase in this case. Figure 5.14 shows the variation of effective normalized diffusivity across a range of particle sizes for volume fractions of the electrolyte of 0.8 and 0.6. The diffusivity ratio used in this case is 0.00133 (see Chapter 2). The resulting effective diffusivity values show a similar trend to that of the effective conductivity. As the particles get smaller for the same volume fraction, the diffusion of Li+ ions through the electrolyte phase is aided because of the increased number of diverse pathways for the diffusion of the ions through the electrolyte. As the particle size decreases from 0.058 to 0.0013, for $\varepsilon_E = 0.8$, there is an increase of 25% in the value of normalized diffusion coefficient as shown in Figure 5.14(a). Similarly, for volume fraction of electrolyte, $\varepsilon_E = 0.6$ as shown in Figure 5.14(b), this increase is almost equal to 53%.

The variation of diffusivity with volume fraction of electrolyte, ε_E for a range of particle sizes, r, is given in Figure 5.15. As expected, increase in the volume fraction of electrolyte increases the diffusivity across all values of r. For instance, in the case of r=0.02, when the electrolyte volume fraction increases from 0.6 to 0.9, there is an almost 97% increase in the diffusivity. This huge increase is expected since at a volume fraction of 0.9, the electrolyte phase occupies 90% of electrode domain. With the decrease in particle size, the rise in diffusivity with volume fraction becomes less steep, i.e., the increase in diffusivity with volume fraction becomes lesser than for bigger particle size. This is because as the particle size decreases, the number of active phase particles increases and the number of ways in which these active phase particles can be distributed throughout the electrode domain decreases. For instance, when the electrolyte volume fraction increases from 0.6 to 0.9 for a particle size of r=0.0013, the increase in diffusivity is nearly 55%. This increase is much less than that for r=0.02 for which, as discussed earlier, the increase in diffusivity is nearly 97%.

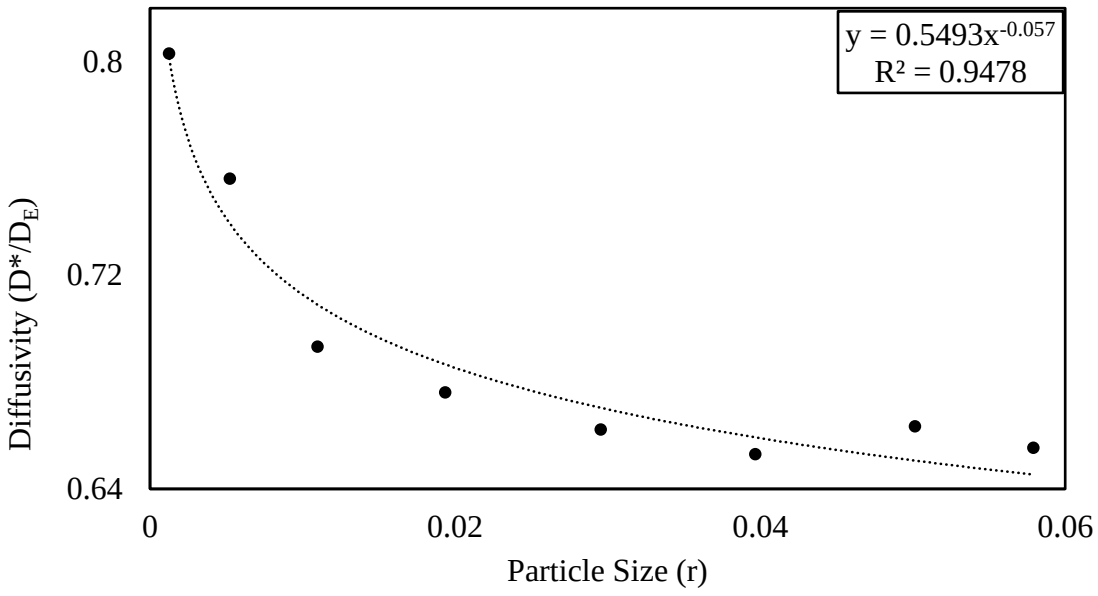

(a)

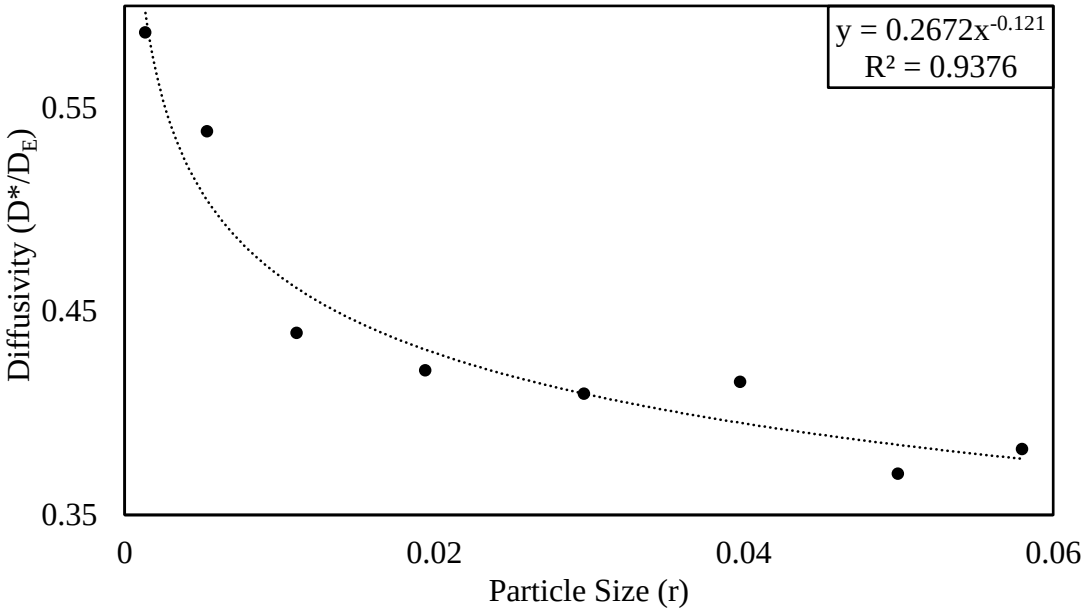

(b)

Figure 5.14: Variation of normalized diffusion coefficient with particle size for (a) $\varepsilon_E = 0.8$ (b) $\varepsilon_E = 0.6$. Dotted lines represent trendlines.

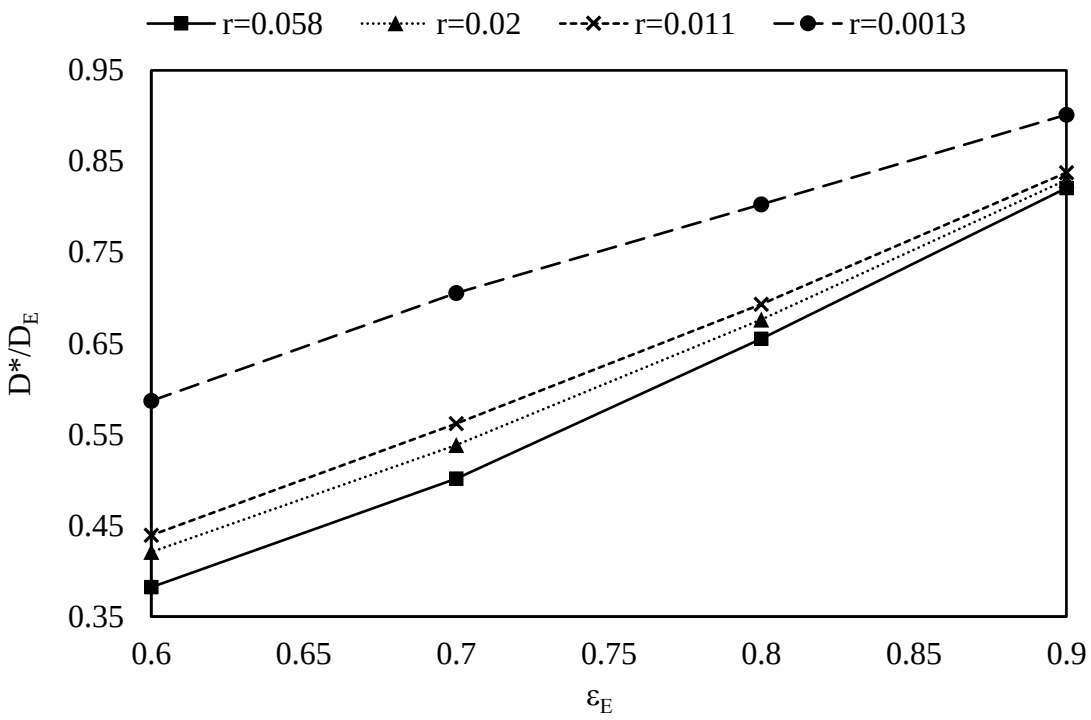

Figure 5.15: Variation of normalized diffusion coefficient with volume fraction of electrolyte phase for different values of particle size.

5.4.2 Evaluation of effective ionic conductivity

Effective ionic conductivity for a porous battery electrode can also be easily evaluated by using the mathematical homogenization method. In this section, few results related to the evaluation of ionic conductivity are provided. Ionic conductivity ratio of 10^{-6} (see Chapter 2) is used to evaluate the effective conductivity values for different microstructures of various volume fractions and particle sizes. For ionic conductivity, like diffusivity, the electrolyte is the dominating phase.

Figure 5.17 shows two different cases of variation of normalized effective ionic conductivity across a range of particle sizes for given volume fractions. For ε_E =0.7, as shown in Figure 5.17(b), the effective ionic conductivity increases by about 40% when the particle size decreases from r=0.058 to r=0.0012. This increase is just about 10% in the case of ε_E =0.9 (see Figure 5.17(a)). Hence, the size of particles does not seem to affect the effective ionic conductivity as drastically for higher volume fractions of the dominating electrolyte phase. This is because when the volume fraction of the dominating phase, electrolyte, increases from 0.7 to 0.9, there is an equivalent reduction in the volume fraction of the active phase particles. At lower volume fraction of the active phase, the number of active particles becomes smaller and they offer much less hindrance to the transport of ions through the electrolyte phase. Hence, in this case, although the decrease in particle size aids the transport of ions by providing more alternative pathways, the effect of particle size decrease on the ionic conductivity is not as significant.

Variation of normalized effective ionic conductivity with volume fraction for a range of particle sizes is given in Figure 5.18. The effective ionic conductivity values increase with an increase in the volume fraction of the dominating electrolyte phase. As in the case of effective diffusivity, the increase is greater for larger particle sizes than for the smaller particle sizes. For instance, when r=0.0013, the increase in ionic conductivity is 55% when the volume fraction of the electrolyte increases from 0.6 to 0.9 whereas it is almost 100% when r=0.058.

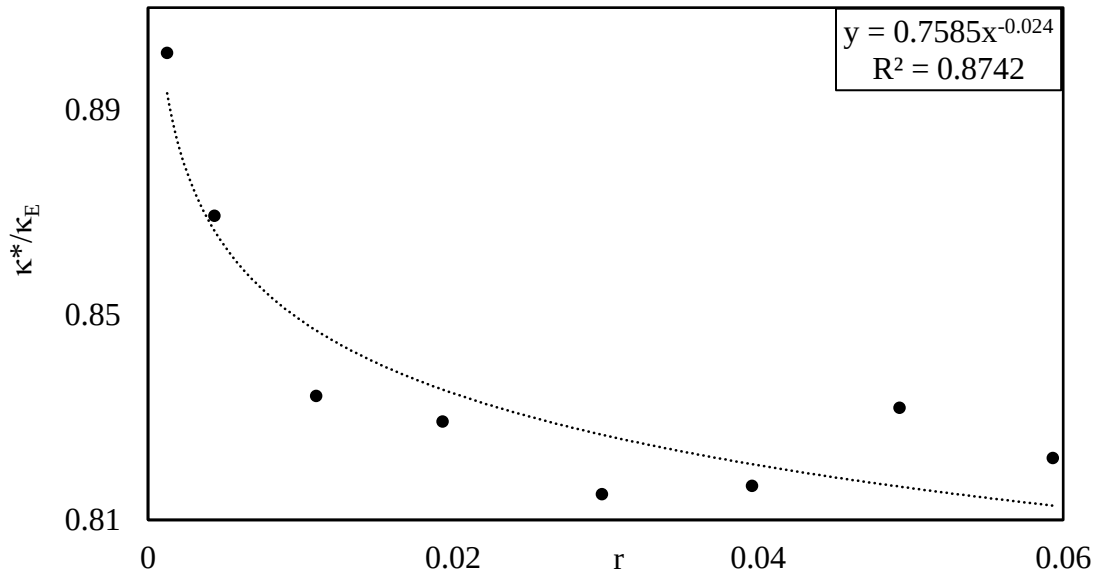

(a)

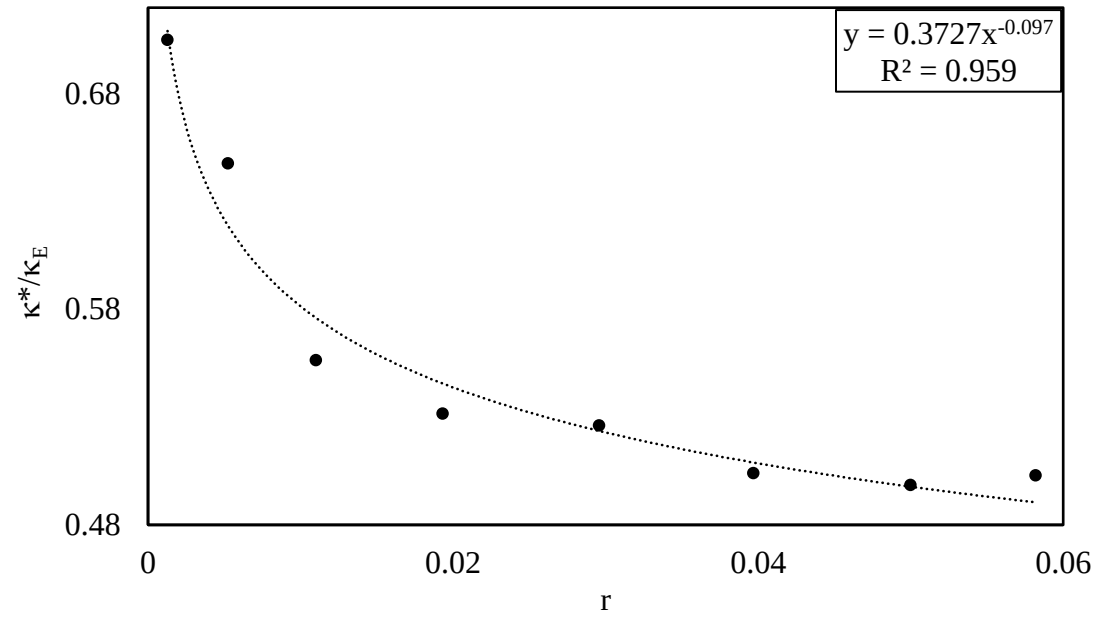

(b)

Figure 5.17: Variation of normalized ionic conductivity with particle size when (a) $\varepsilon_E = 0.9$ (b) $\varepsilon_E = 0.7$. Dotted lines represent trendlines.

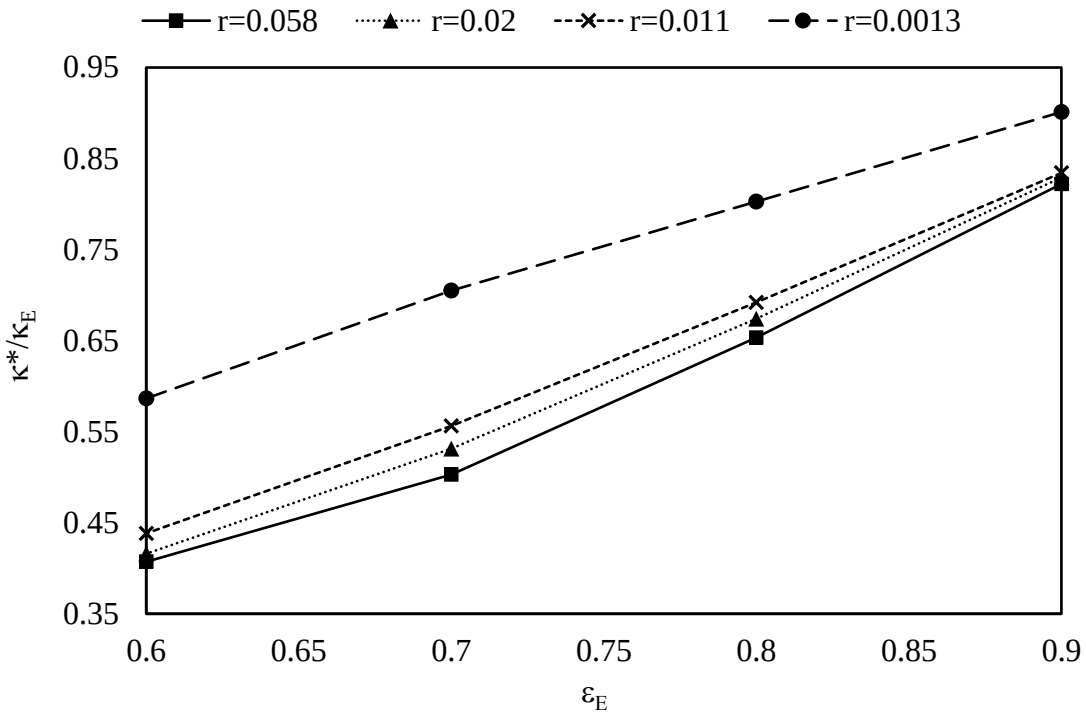

Figure 5.18: Variation of normalized ionic conductivity with volume fraction of electrolyte phase for different values of particle size.

5.5 Evaluation of Tortuosity

The concept of tortuosity, τ is used in literature to express the decrease in effective transport properties of a macroscopic composite [55]. It is an important parameter used extensively in research community in order to evaluate the performance of lithium ion battery electrodes [56]. However, there is inconsistency in how tortuosity is defined across literature [36, 55–57].

In this research work, tortuosity, τ, is defined as the effective geometric parameter that is related to porosity and effective electronic conductivity, ionic diffusivity and ionic conductivity by [5,25,58] :

$$\sigma^* = \sigma\frac{\varepsilon_{AP}}{\tau}, \quad D^* = D\frac{\varepsilon_E}{\tau}, \quad \kappa^* = \kappa\frac{\varepsilon_E}{\tau}. \tag{5.12}$$

In essence, the value of tortuosity provides an indication of how difficult the path for the transport of the species is through a microstructure geometry because of the presence of more than one phase.

For conductive pathways which are parallel to the transport direction with no barriers to transport, a value of τ = 1 can be assumed. In case of li-ion battery electrodes, the microstructures are complicated and values of τ are generally greater than 1 which indicates that the conductive pathways are tortuous. This means that the effective electric conductivity values are always lower than that of the actual conductivity of the conductive phase [5].

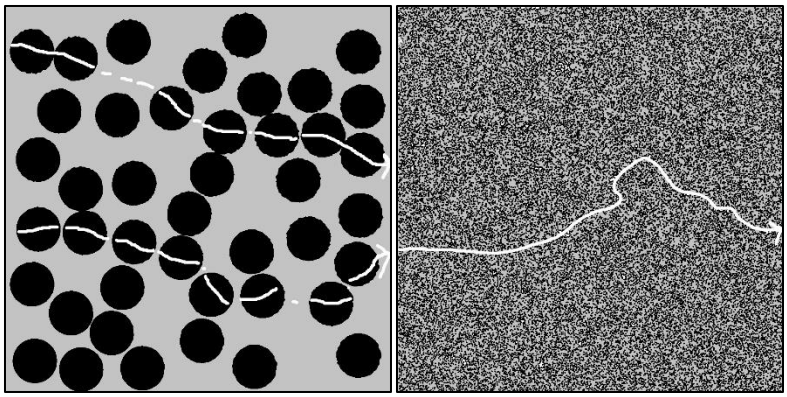

(a) (b)

Figure 5.19: Schematic representation of tortuosity related to effective electrical conductivity for ε_{AP} = 0.45 with (a) r=0.06 and (b) r=0.0013. The white lines with arrowheads indicate the paths the electrons may use to travel across the electrode microstructure.

Figures 5.19 and 5.20 illustrate the concept of tortuosity in terms of its relationship with porosity and effective transport properties. In Figure 5.19, two different representative microstructure images of the same volume fraction of active particles (ε_{AP} = 0.45) but with different particle sizes are shown. The white lines with arrowheads represent the potential electron transport paths. Smaller particles are randomly spread throughout the microstructure domain increasing the potential pathways for the electrons to transport compared to the domain with larger particles. Hence, the first microstructure is more tortuous for the transport of electrons. Similarly, Figure 5.20 illustrates the tortuosity for the transport of lithium ions (diffusion) for two different microstructures with same volume fraction but different particle sizes. In this case, the smaller particle size of active particles creates more difficulty for the transport of ions through the electrolyte leading to a higher value of tortuosity.

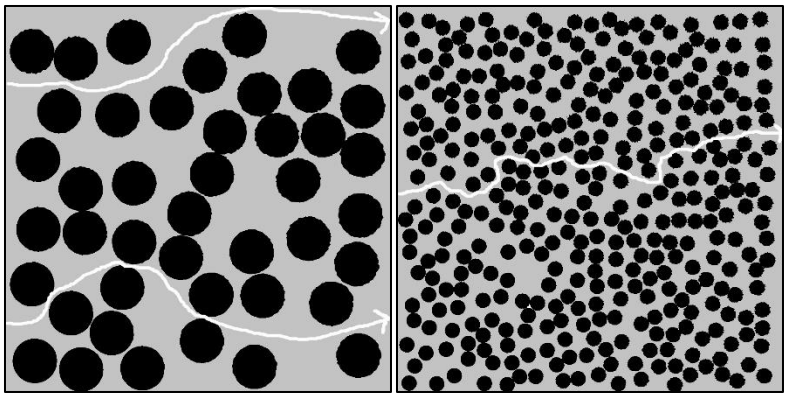

Figure 5.20: Schematic representation of tortuosity related to effective diffusivity for ε_{AP} = 0.45 with (a) r=0.06 and (b) r=0.02. The white lines with arrowheads indicate the paths the electrons may use to travel across the electrode microstructure.

Based on Bruggeman's postulates, the relationship between τ and ε_{AP} from Equation (5.12) for the case of effective conductivity can be restated as:

$$\tau = \varepsilon_{AP}^{-0.5}. \tag{5.13}$$

From this definition, the value of $\tau = 1$ gives a value of $\varepsilon_{AP} = 1$. This is equivalent to the entire microstructure domain being filled with the conductive phase. However, the presence of a second phase means that this is not possible. Thorat et al. [5] provided a generalized form of Bruggeman's relation to relate tortuosity with the volume fraction as

$$\tau = c\varepsilon_{AP}^{1-\gamma}. \tag{5.14}$$

Most of the research work in this field is carried out by using Equation (5.13) which can be obtained by setting the value of $c = 1$ and $\gamma = 1.5$ in Equation (5.14) [5]. Figure 5.21

shows the comparison between tortuosity and volume fraction of the solid conductive phase for different particle sizes for the case of effective electrical conductivity. It must be noted that the values of tortuosity based on Bruggeman's formula are the same for different particle sizes for a given value of ε_{AP}. To better understand the role of the solid phase particle size r on the value of τ, a detailed analysis is presented for the case of $\varepsilon_{AP} = 0.3$ as summarized in Table 5.3. For this fixed volume fraction, as the particle size increases from r = 0.001 to r = 0.05, there is a thirteen-fold increase in the value of τ. This is not unexpected since there is a considerable variation in the microstructure topology between these two particle sizes. Smaller particle size for the same given volume fraction leads to more active particles for electrical conduction. On the other hand, as the particle size increases, the number of active particles distributed throughout the electrode is much less. This means there are significantly fewer pathways for the transport of electrons leading to a higher value of τ, i.e., a more tortuous path for the electrons to move. Although Equation (5.13) provides a limiting lower value of τ to be 1, the values of τ are smaller than 1 in case of

Table 5.3: Variation of τ and corresponding values of coefficients c and γ for different values of r.

r	**c**	**γ**	**τ ($\varepsilon_{AP} = 0.3$)**
0.05	5.2394	1.4901	9.4525
0.01	2.3170	1.2824	3.2553
0.001	0.7209	1.0346	0.7516

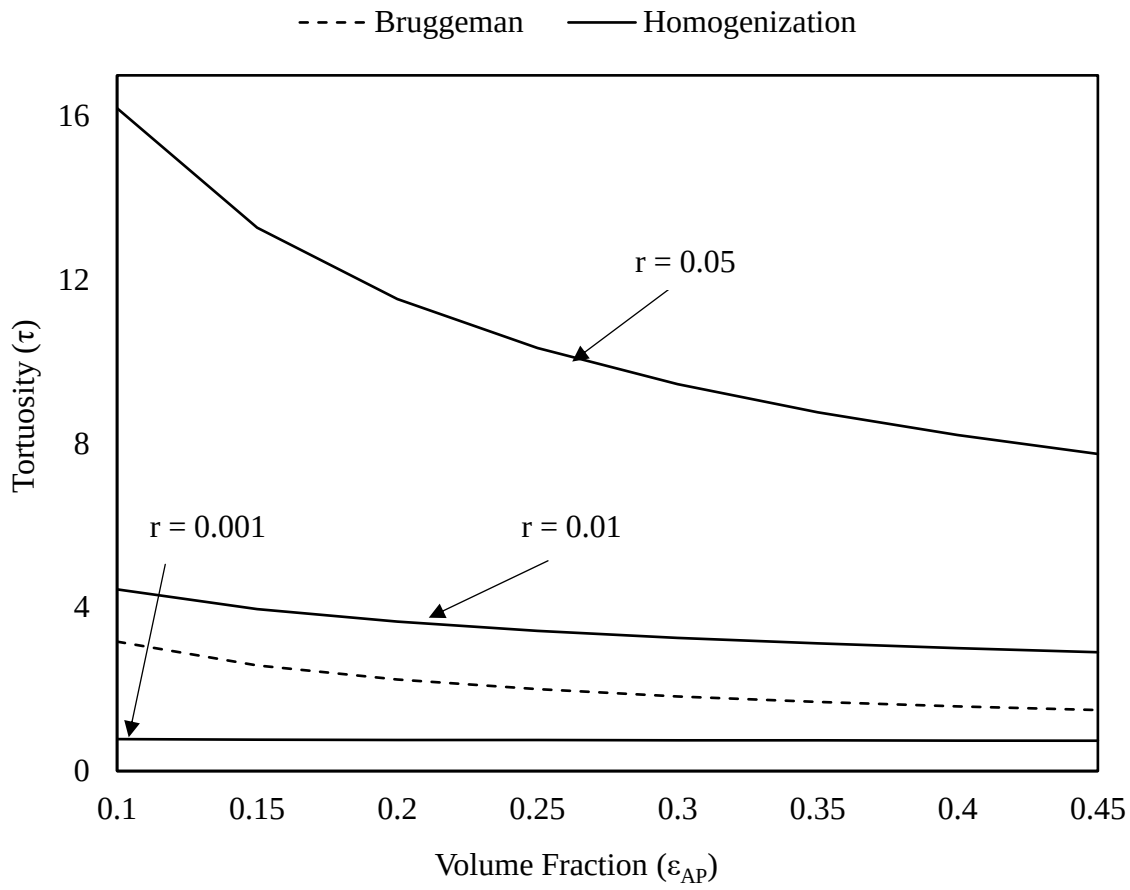

Figure 5.21: Comparison of tortuosity vs volume fraction for different radii based on the mathematical homogenization method with Bruggeman's formula for different microstructures with different radii for h = 10^7.

r = 0.001 as shown in Figure 5.21. This is consistent with the findings of Hutzenlaub et al.[45] who also reported values of τ much smaller than 1 for a reconstructed $LiCoO_2$ li-ion battery cathode. Similarly, Cussler [59] reported values of tortuosity measured for diffusivity to be as high as 10.

Using the structure of Equation (5.14), we can obtain the values of the constants c and Bruggeman's exponent γ for each value of r as summarized in Table 5.3. It is evident that

these expressions are very different from the one given in Equation (5.13). Kehrwald et al. [57] also report similar differences between their derived expressions and the one described by Bruggeman's relation. Also, with an increase in the volume fraction of the conductive phase, there is an increase in the possible conductive pathways for the electrons to travel. Hence, with the increase in the values of ε_{AP}, the values of τ decrease for all the cases shown in Figure 5.21.

PART II: Discharge Characteristics

In this part, the results and analysis of the study of the influence of microstructure geometry discharge properties are presented.

5.6 Effect of Microstructure Geometry on Discharge Characteristics

In this section, effective properties of different Li-ion cell electrode microstructures based on various parameters are evaluated which are then used to study the influence of microstructure geometry on the discharge characteristics of an idealized li-ion cell. Comparison of discharge characteristics of the cell based on the evaluation of effective properties between the traditionally used Bruggeman's method and homogenization method is also carried out. In doing so, the influence of microstructure on cell discharge characteristics using the P2D model is discussed. The aim is to highlight the importance of accurate prediction of effective properties based on microstructure geometry using the proposed formulation and to study the limitation of Bruggeman's formula on battery performance prediction.

Schematic diagram model of Li-ion battery considered for study is shown in Figure 4.5. The electrodes are assumed to have two distinct phases viz. electrolyte and active phase. The electrolyte material is $LiPF_6$ salt dissolved in organic solvent 1:2 v/v mixture of EC: DMC with the polymer matrix , p(VdF-HFP) [25]. The negative and positive electrodes are composed of carbon-based material and $Li_xMn_2O_4$ respectively. Table 5.4

summarizes the values of different parameters used in this study. All key parameters including the properties of electrodes and electrolyte used here are from Ref. [25]. Tables I-1 , I-2 and I-3 provided in APPENDIX include the parameters for simulation used to evaluate the discharge characteristics. More information on charge and discharge cycles, SOC and equilibrium potentials can be found in COMSOL's documentation [48].

Electrical conductivity of electrolyte is assumed to be 10^{-8} which gives a conductivity ratio, h of nearly 10^{8} and 10^{10} for positive and negative electrodes respectively. Although this value is generally assumed to be zero in literature, the described homogenization method does not allow us to consider a value of zero [3]. However, it is sufficiently small as compared to the values of electrical conductivity of active particles used in this study so as to render the effect of this assumption negligible. Ionic conductivity of electrolyte depends on the salt concentration, temperature and solvent ratio of EC/DMC [25].

Table 5.4: Key parameters for the electrodes.

Parameter	**Positive electrode**	**Negative Electrode**
Active Material	$Li_xMn_2O_4$	Li_xC_6
L *	174 μm	100 μm [25]
σ_{AP}	3.8 S/m	100 S/m [25]
r_p	8.5 μm	12.5 μm [25]
ε_{AP}	0.3	0.45
ε_E	0.7	0.55
h	3.8×10^{8}	10^{10}

**The width of separator is 52 μm.*[25]

Here, only the electrode conductivity is modified using the proposed homogenization based formulation and the results are compared with the electrode conductivity based on the correction given by Bruggeman's formula. Bruggeman's formula is used for the correction of ionic conductivity and diffusion in all the cases. For simulation, MUMPS solver available in COMSOL is used [48].

Figure 5.22 shows the discharge curves at the discharge rates of 1C, 2C, 4C and 8C using the effective conductivity values of both positive and negative electrodes based on Bruggeman's formula and the proposed homogenization-based formulation. The C-rate provides a measure of the rate of discharge of battery relative to its maximum capacity. 1C discharge rate here is the current density which when applied discharges the cell in an hour. The theoretical 1C-rate current density in this case is 17.5 A/m^2 [25]. As the discharge rate increases from 1C to 8C, the discharge capacity decreases at an increasing rate for a given cell voltage. For a cell voltage of 3V, the cell discharge capacity decreases by 65% at a discharge rate of 8C as compared to that at 1C based on Bruggeman's estimate. However, the change in discharge capacity is 69% when the homogenization based formulation is used. At 8C, the 3V discharge capacity of the cell is almost 14% lower based on homogenization approach as compared to Bruggeman's formula. This difference in discharge capacities at different cell voltage values increases with increasing discharge rate as shown in Figure 5.22. This highlights the need for the use of microstructure geometry information while evaluating the effective properties.

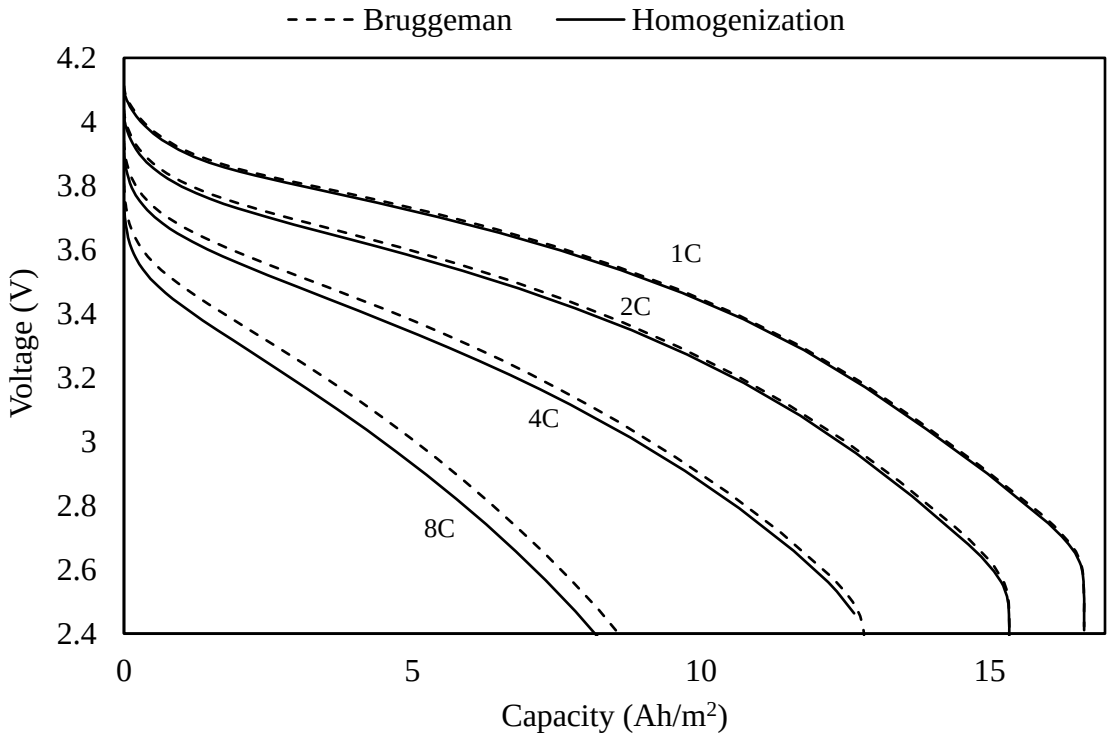

Figure 5.22: Discharge curves evaluated at different discharge rates. The solid lines represent the curves based on the effective electrical conductivity of electrodes evaluated using the proposed formulation and the dotted lines indicate the curves based on the Bruggeman's effective electric conductivity prediction.

Figure 5.23 shows the variation of discharge characteristics with the change in the active particle sizes for both positive and negative electrodes at different discharge rates. Three different cases are summarized in Table 5.5, and account for three different particles sizes.

Table 5.5 also includes the values of the Bruggeman's exponent (γ) that should be used based on the homogenization formulation instead of the idealized value of γ=1.5. For

Table 5.5: Different cases with variation of active particle sizes and corresponding values of effective electrical conductivity and Bruggeman's exponent.

	Positive Electrode			**Negative Electrode**		
Case	**r_p (µm)**	**σ*(S/m)**	**γ**	**r_n (µm)**	**σ*(S/m)**	**γ**
A	42.5	0.037	3.842	62.5	1.008	5.758
B	8.5	0.115	2.903	12.5	2.921	4.425
C	1.7	0.341	2.001	2.5	8.162	3.138

example, for case A, γ is 3.842 which is more than twice the value proposed by Bruggeman's formula. Previous studies have also used higher values of γ [25].

Decrease in particle size for the same values of volume fraction corresponds to an increase in the number of active particles. This leads to greater number of pathways for electronic conduction and hence better discharge characteristics are observed. For instance, the value of discharge capacity for a cell voltage of 3V at the discharge rate of 1C increases by almost 80% as the active particle sizes for both electrodes are decreased by 25% (cases A and C) based on the homogenization based formulation. Also, as discussed earlier, the difference between the discharge characteristic curves based on homogenization and Bruggeman's formula increases with the increase in discharge rates as shown in Figure 5.23 (a & b). Again, an increase in the volume fraction means that there is a greater amount of active materials available for conduction. This increase in the amount of active materials

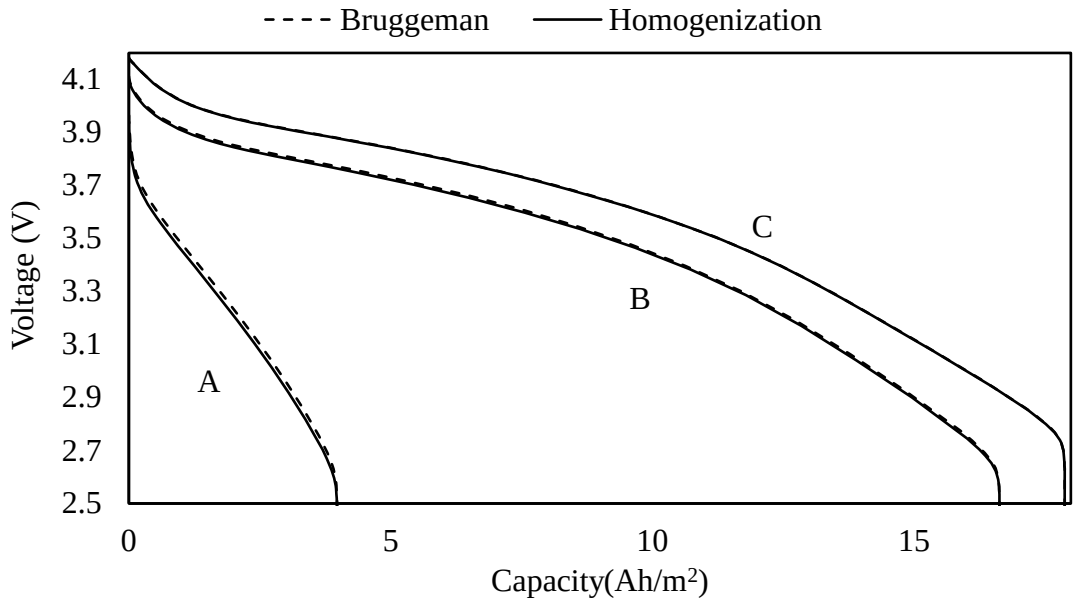

(a)

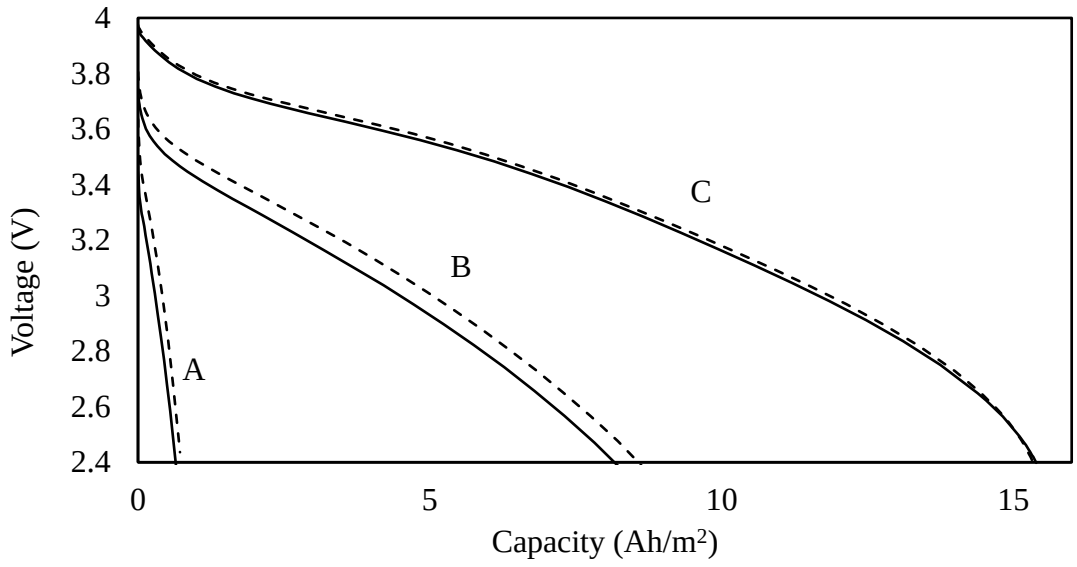

(b)

Figure 5.23: Discharge curves evaluated for different particle size of electrode active materials at discharge rate of (a) 1C (b) 8C.

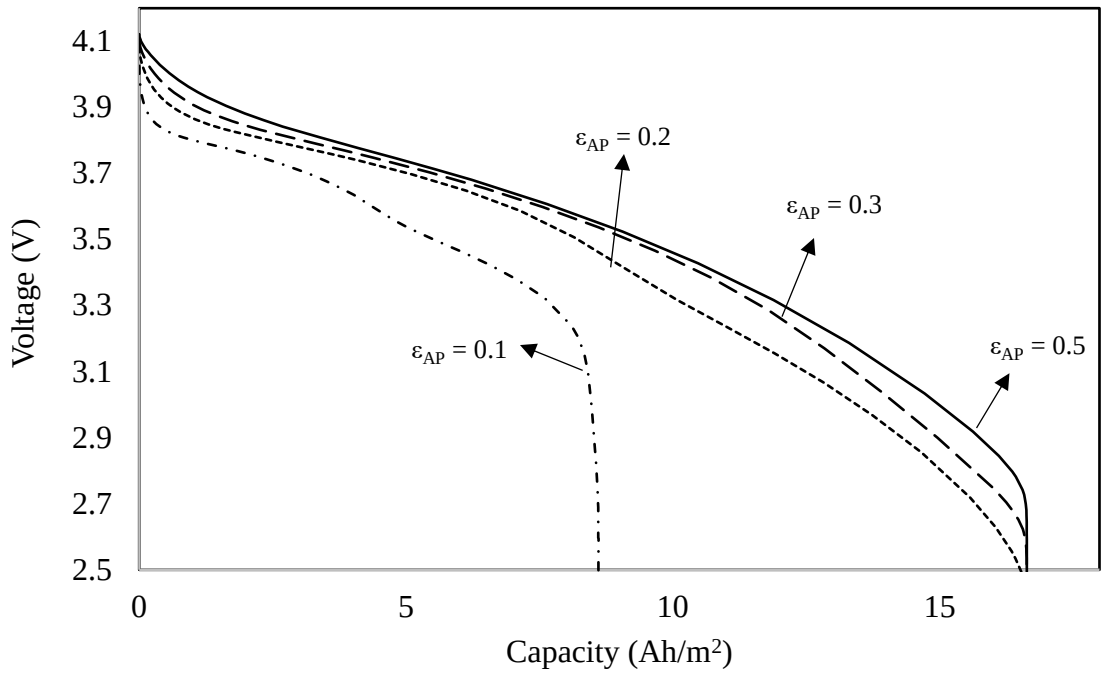

Figure 5.24: Discharge curves at 1C evaluated for different volume fractions of active particles of positive electrode for particle size and conductivity ratio given in Case B. Negative electrode and electrolyte properties are kept unchanged from Case B.

leads to better discharge characteristics. Figure 5.24 shows the discharge curves for different values of volume fraction and corresponding effective electrode conductivity for the positive electrode only using the proposed formulation at a discharge rate of 1C. As the volume fraction of the active particles in the positive electrode increases, a considerable improvement in the discharge characteristics is observed. For instance, the 3V cell voltage capacity increases by 76% as the volume fraction of the active particles increases from 0.1 to 0.5. Figure 5.25 shows the discharge characteristics comparison between the results

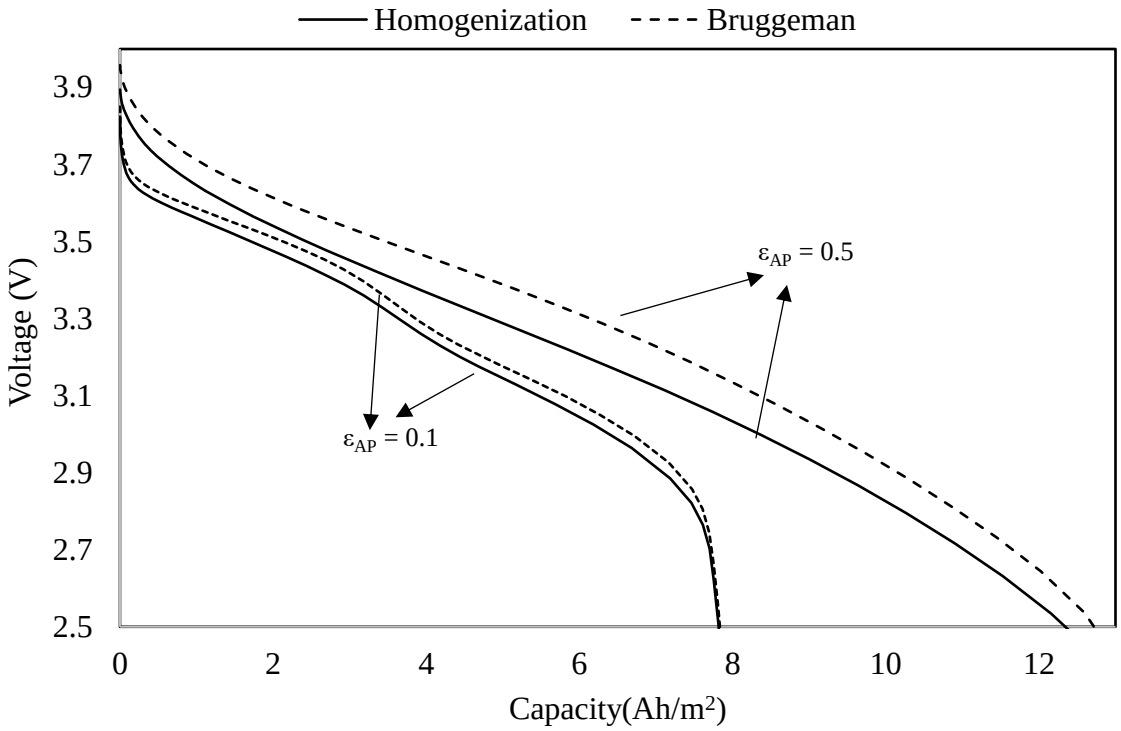

Figure 5.25: Comparison of discharge curves based on effective conductivity estimated using proposed homogenization formulation and Bruggeman's formula at 1C evaluated for different volume fractions of active particles of positive electrode for particle size and conductivity ratio given in Case B. Negative electrode and electrolyte properties are kept unchanged from Case B.

based on proposed formulation and Bruggeman's theory for different volume fractions. The difference in the discharge characteristics is higher for a higher active particle volume fraction $\varepsilon_{AP} = 0.5$ as compared to $\varepsilon_{AP} = 0.1$ in both cases. However, for both values of volume fraction, Bruggeman's theory based effective conductivity value overpredicts the voltage at a given discharge capacity.

Chapter 6

CONCLUSION AND RECOMMENDATIONS

In this research work, an extensive analysis of the effective electrical conductivity of randomly generated microstructures idealized for Li-ion battery electrodes was carried out by employing a mathematical homogenization method. The results obtained based on this approach were then compared with the famous Bruggeman's formula. The Bruggeman's formula fails to account for the microstructure geometry and so it always predicts a constant value of effective conductivity based only on the volume fraction of conductive phase. However, with the mathematical homogenization technique, when the microstructure geometry is considered, we observe variations in the value of effective conductivity. In other words, using mathematical homogenization, we can determine the effective conductivity as a function of the microstructure.

Based on the results obtained from the mathematical homogenization method, an explicit formula relating effective conductivity with conductivity ratio of phases, particle size and volume fraction of active phase has been proposed. The aim is to provide a simple method for the evaluation of effective electrical conductivity of the additive-free electrode of a Li-ion battery based on the conducting solid phase and non-conducting electrolyte phase. An analysis of the proposed formulation was also carried out. For two hundred different cases analyzed using the formula, average relative error of approximately 8% was

observed between the actual values based on homogenization method and the proposed formula for a mono-modal particle size distribution.

An application of the proposed formulation was demonstrated by studying the discharge characteristics of a Li-ion battery based on the P2D model. The differences in the discharge curves was highlighted by comparing the results when the microstructural effect is considered (by employing the mathematical homogenization to determine the effective conductivity) and when it is ignored (by employing the Bruggeman's formula for calculating the effective conductivity), respectively. The results showed that this variation is significant at higher discharge rates and for higher volume fraction of active particles.

It can be concluded that by incorporating multiple phases in the analysis, we could obtain more insights and a more rigorous formulation to accurately evaluate the effective electrical conductivity. Additionally, particle size distribution based evaluation of effective diffusion coefficient and ionic conductivity of electrolyte could also be considered to provide a better insight into the limitations of Bruggeman's formula and could yield a more accurate representation of the performance characteristics of a Li-ion battery. Similarly, use of a more realistic representation of the microstructure by incorporating the information on particle polydispersity could provide better insights into the effective properties of the electrodes.

REFERENCES

[1] J. Lu, Z. Chen, Z. Ma, F. Pan, L. A. Curtiss, and K. Amine, "The role of nanotechnology in the development of battery materials for electric vehicles," *Nat. Nanotechnol.*, vol. 11, no. 12, pp. 1031–1038, Dec. 2016.

[2] V. Ramadesigan, P. W. C. Northrop, S. De, S. Santhanagopalan, R. D. Braatz, and V. R. Subramanian, "Modeling and Simulation of Lithium-Ion Batteries from a Systems Engineering Perspective," *J. Electrochem. Soc.*, vol. 159, no. 3, pp. R31–R45, Jan. 2012.

[3] A. Gully, H. Liu, S. Srinivasan, A. K. Sethurajan, S. Schougaard, and B. Protas, "Effective Transport Properties of Porous Electrochemical Materials -- A Homogenization Approach," *J. Electrochem. Soc.*, vol. 161, no. 8, pp. E3066–E3077, Apr. 2014.

[4] D. A. G. Bruggeman, "Berechnung verschiedener physikalischer Konstanten von heterogenen Substanzen. I. Dielektrizitätskonstanten und Leitfähigkeiten der Mischkörper aus isotropen Substanzen," *Ann. Phys.*, vol. 416, no. 7, pp. 636–664, Jan. 1935.

[5] I. V. Thorat, D. E. Stephenson, N. A. Zacharias, K. Zaghib, J. N. Harb, and D. R. Wheeler, "Quantifying tortuosity in porous Li-ion battery materials," *J. Power Sources*, vol. 188, no. 2, pp. 592–600, Mar. 2009.

[6] P. Gerland, A. Raftery, H. Ševčíková, N. Li, and D. Gu, "World population stabilization unlikely this century," 2014.

[7] U.S. Energy Information Administration, "International Energy Outlook 2016," 2016.

[8] NOAA, "Trends in Atmospheric Carbon Dioxide," *US Department of Commerce*, 2017. [Online]. Available: https://www.esrl.noaa.gov/gmd/ccgg/trends/index.html. [Accessed: 16-Aug-2017].

[9] NASA and NOAA, "NASA, NOAA Data Show 2016 Warmest Year on Record Globally," 2017. [Online]. Available: https://www.nasa.gov/press-release/nasa-noaa-data-show-2016-warmest-year-on-record-globally. [Accessed: 16-Aug-2017].

[10] Environment and Climate Change Canada, "Canadian Environmental Sustainability Indicators : Greenhouse Gas Emissions," 2017.

[11] US E.P.A, "Inventory of U.S. Greenhouse Gas Emissions and Sinks: 1990-2015," 2017.

[12] European Renewable Energy Council(EREC), "Re-thinking 2050," 2010.

[13] H. Ibrahim, A. Ilinca, and J. Perron, "Energy storage systems—Characteristics and

comparisons," *Renew. Sustain. Energy Rev.*, vol. 12, no. 5, pp. 1221–1250, Jun. 2008.

[14] T. Sasaki, Y. Ukyo, and P. Novák, "Memory effect in a lithium-ion battery," *Nat Mater*, vol. 12, no. 6, pp. 569–575, Jun. 2013.

[15] J. Lu, Z. Chen, Z. Ma, F. Pan, L. A. Curtiss, and K. Amine, "The role of nanotechnology in the development of battery materials for electric vehicles," *Nat. Nanotechnol.*, vol. 11, no. 12, pp. 1031–1038, Dec. 2016.

[16] M. R. Palacín, "Recent advances in rechargeable battery materials: a chemist's perspective," *Chem. Soc. Rev.*, vol. 38, no. 9, p. 2565, Aug. 2009.

[17] Y. Nishi, "The development of lithium ion secondary batteries," *Chem. Rec.*, vol. 1, no. 5, pp. 406–413, Jan. 2001.

[18] J. B. Dunn, L. Gaines, M. Barnes, J. L. Sullivan, and M. Wang, "Material and Energy Flows in the Materials Production, Assembly, and End-of-Life Stages of the Automotive Lithium-Ion Battery Life Cycle," Argonne, IL (United States), Jan. 2014.

[19] R. D. Pal and A. K. R. Paul, "Charge-discharge studies of lithium-ion batteries."

[20] M. Park, X. Zhang, M. Chung, G. B. Less, and A. M. Sastry, "A review of conduction phenomena in Li-ion batteries," *J. Power Sources*, vol. 195, pp. 7904–7929, 2010.

[21] L. O. Valøen and J. N. Reimers, "Transport Properties of LiPF[sub 6]-Based Li-Ion Battery Electrolytes," *J. Electrochem. Soc.*, vol. 152, no. 5, p. A882, May 2005.

[22] A. Seaman, T.-S. Dao, and J. Mcphee, "A survey of mathematics-based equivalent-circuit and electrochemical battery models for hybrid and electric vehicle simulation," *J. Power Sources*, vol. 256, pp. 410–423, 2014.

[23] V. Ramadesigan, P. W. C. Northrop, S. De, S. Santhanagopalan, R. D. Braatz, and V. R. Subramanian, "Modeling and Simulation of Lithium-Ion Batteries from a Systems Engineering Perspective," *J. Electrochem. Soc.*, vol. 159, no. 3, pp. R31–R45, Jan. 2012.

[24] N. T. Tran, M. Vilathgamuwa, T. Farrell, and S. S. Choi, "Matlab simulation of lithium ion cell using electrochemical single particle model," in *2016 IEEE 2nd Annual Southern Power Electronics Conference (SPEC)*, 2016, pp. 1–6.

[25] M. Doyle, J. Newman, A. S. Gozdz, C. N. Schmutz, and J. Tarascon, "Comparison of Modeling Predictions with Experimental Data from Plastic Lithium Ion Cells," *J. Electrochem. Soc.*, vol. 143, no. 6, p. 1890, Jun. 1996.

[26] J. Newman and W. Tiedemann, "Porous-electrode theory with battery

applications," *AIChE J.*, vol. 21, no. 1, pp. 25–41, Jan. 1975.

[27] A. Jokar, B. Rajabloo, M. D. Esilets, and M. Lacroix, "Review of simplified Pseudo-two-Dimensional models of lithium-ion batteries," *J. Power Sources*, vol. 327, pp. 44–55, 2016.

[28] H. Zheng, R. Yang, G. Liu, X. Song, and V. S. Battaglia, "Cooperation between Active Material, Polymeric Binder and Conductive Carbon Additive in Lithium Ion Battery Cathode," *J. Phys. Chem. C*, vol. 116, no. 7, pp. 4875–4882, Feb. 2012.

[29] S. W. Peterson and D. R. Wheeler, "Direct Measurements of Effective Electronic Transport in Porous Li-Ion Electrodes," *J. Electrochem. Soc.*, vol. 161, no. 14, pp. A2175–A2181, Jan. 2014.

[30] Y.-H. Chen, C.-W. Wang, G. Liu, X.-Y. Song, V. S. Battaglia, and A. M. Sastry, "Selection of Conductive Additives in Li-Ion Battery Cathodes," *J. Electrochem. Soc.*, vol. 154, no. 10, p. A978, Oct. 2007.

[31] D.-H. Ha, T. Ly, J. M. Caron, H. Zhang, K. E. Fritz, and R. D. Robinson, "A General Method for High-Performance Li-Ion Battery Electrodes from Colloidal Nanoparticles without the Introduction of Binders or Conductive-Carbon Additives: The Cases of MnS, Cu $_{2-x}$ S, and Ge," *ACS Appl. Mater. Interfaces*, vol. 7, no. 45, pp. 25053–25060, Nov. 2015.

[32] C. Liu, Z. G. Neale, and G. Cao, "Understanding electrochemical potentials of cathode materials in rechargeable batteries," *Biochem. Pharmacol.*, vol. 19, no. 2, pp. 109–123, 2016.

[33] J. W. Fergus, "Recent developments in cathode materials for lithium ion batteries," *J. Power Sources*, vol. 195, no. 4, pp. 939–954, Feb. 2010.

[34] D. Y. W. Yu, K. Yanagida, Y. Kato, and H. Nakamura, "Electrochemical Activities in Li2MnO3," *J. Electrochem. Soc.*, vol. 156, no. 6, pp. A417–A424, Jun. 2009.

[35] N. Yabuuchi, K. Kubota, Y. Aoki, and S. Komaba, "Understanding Particle-Size-Dependent Electrochemical Properties of Li_2MnO_3-Based Positive Electrode Materials for Rechargeable Lithium Batteries," *J. Phys. Chem. C*, vol. 120, no. 2, pp. 875–885, Jan. 2016.

[36] D.-W. Chung, M. Ebner, D. R. Ely, V. Wood, and R. Edwin García, "Validity of the Bruggeman relation for porous electrodes," *Model. Simul. Mater. Sci. Eng.*, vol. 21, no. 7, p. 74009, Oct. 2013.

[37] S. T. Taleghani, B. Marcos, K. Zaghib, and G. Lantagne, "A Study on the Effect of Porosity and Particles Size Distribution on Li-Ion Battery Performance," *J. Electrochem. Soc.*, vol. 164, no. 11, pp. E3179–E3189, May 2017.

[38] R. E. García, Y.-M. Chiang, W. Craig Carter, P. Limthongkul, and C. M. Bishop, "Microstructural Modeling and Design of Rechargeable Lithium-Ion Batteries," *J. Electrochem. Soc.*, vol. 152, no. 1, p. A255, Jan. 2005.

[39] D.-W. Chung, P. R. Shearing, N. P. Brandon, S. J. Harris, and R. E. Garcia, "Particle Size Polydispersity in Li-Ion Batteries," *J. Electrochem. Soc.*, vol. 161, no. 3, pp. A422–A430, Jan. 2014.

[40] A. Vadakkepatt, B. Trembacki, S. R. Mathur, and J. Y. Murthy, "Bruggeman's Exponents for Effective Thermal Conductivity of Lithium-Ion Battery Electrodes," *J. Electrochem. Soc.*, vol. 163, no. 2, pp. A119–A130, Nov. 2016.

[41] B. Yan, C. Lim, L. Yin, and L. Zhu, "Three Dimensional Simulation of Galvanostatic Discharge of LiCoO2 Cathode Based on X-ray Nano-CT Images," *J. Electrochem. Soc.*, vol. 159, no. 10, pp. A1604–A1614, Aug. 2012.

[42] P. K. Samantray, P. Karthikeyan, and K. S. Reddy, "Estimating effective thermal conductivity of two-phase materials," *Int. J. Heat Mass Transf.*, vol. 49, no. 21–22, pp. 4209–4219, Oct. 2006.

[43] C.-W. Wang, A. M. Sastry, K. A. Striebel, and K. Zaghib, "Extraction of Layerwise Conductivities in Carbon-Enhanced, Multilayered LiFePO 4 Cathodes," 2005.

[44] D. Guy, B. Lestriez, R. Bouchet, and D. Guyomard, "Critical Role of Polymeric Binders on the Electronic Transport Properties of Composites Electrode," *J. Electrochem. Soc.*, vol. 153, no. 4, p. A679, Apr. 2006.

[45] T. Hutzenlaub, S. Thiele, and R. Zengerle, "Three-dimensional reconstruction of a LiCoO2 Li-ion battery cathode," *Electrochem. Solid*, 2011.

[46] Y.-H. Chen, C.-W. Wang, X. Zhang, and A. M. Sastry, "Porous cathode optimization for lithium cells: Ionic and electronic conductivity, capacity, and selection of materials," *J. Power Sources*, vol. 195, pp. 2851–2862, 2010.

[47] S. Torquato, *Random heterogeneous materials: microstructure and macroscopic properties*, vol. 16. Springer Science & Business Media, 2013.

[48] COMSOL Inc., "COMSOL Multiphysics Modeling Software." .

[49] Kun Lee and Dongsuk Kum, "The impact of inhomogeneous particle size distribution on Li-ion cell performance under galvanostatic and transient loads," in *2016 IEEE Transportation Electrification Conference and Expo, Asia-Pacific (ITEC Asia-Pacific)*, 2016, pp. 454–459.

[50] The MathWorks Inc., "Image Processing Toolbox - MATLAB." .

[51] P. Castaneda, "Bounds and estimates for the properties of nonlinear heterogeneous systems," *Trans. R. Soc. ...*, 1992.

[52] K. Golden, “Bounds on the complex permittivity of a multicomponent material,” *J. Mech. Phys. Solids*, vol. 34, no. 4, pp. 333–358, Jan. 1986.

[53] Kun Lee and Dongsuk Kum, “The impact of inhomogeneous particle size distribution on Li-ion cell performance under galvanostatic and transient loads,” in *2016 IEEE Transportation Electrification Conference and Expo, Asia-Pacific (ITEC Asia-Pacific)*, 2016, pp. 454–459.

[54] R. Darling and J. Newman, “Modeling a Porous Intercalation Electrode with Two Characteristic Particle Sizes,” *J. Electrochem. Soc.*, vol. 144, no. 12, p. 4201, Dec. 1997.

[55] M. Ebner, D.-W. Chung, R. E. García, and V. Wood, “Tortuosity Anisotropy in Lithium-Ion Battery Electrodes,” *Adv. Energy Mater.*, vol. 4, no. 5, p. 1301278, Apr. 2014.

[56] M. Ebner and V. Wood, “Tool for Tortuosity Estimation in Lithium Ion Battery Porous Electrodes,” *J. Electrochem. Soc.*, vol. 162, no. 2, pp. A3064–A3070, Dec. 2014.

[57] D. Kehrwald, P. Shearing, and N. Brandon, “Local tortuosity inhomogeneities in a lithium battery composite electrode,” *Electrochem. …*, 2011.

[58] C.-F. Chen, A. Verma, and P. P. Mukherjee, “Probing the Role of Electrode Microstructure in the Lithium-Ion Battery Thermal Behavior,” *J. Electrochem. Soc.*, vol. 164, no. 11, pp. E3146–E3158, May 2017.

[59] E. L. Cussler, *Diffusion : mass transfer in fluid systems*. Cambridge University Press, 2009.

APPENDIX: COMSOL SIMULATION PARAMETERS

Table I-1: Properties of LMO electrode, $LiMn_2O_4$ spinel (Positive electrode).

Property	Value
Reference Concentration	22860 mol/m^3
Maximum electrode state of charge (SOC_{max})	0.995
Minimum electrode state of charge (SOC_{min})	0.175
Density	4140 kg/ m^3
Reference temperature, T_ref	298 K
Anodic Transfer Coefficient, α_a	0.5
Cathodic Transfer Coefficient, α_c	0.5
Electrolyte Reference Concentration	1 mol/m^3
Reaction Rate Coefficient (anodic, k_a and cathodic, k_c)	2×10^{-11} m/s
Initial Species (particles) Concentration	3900 mol/m^3

Table I-2: Properties of graphite anode (Negative electrode).

Property	**Value**
Maximum electrode state of charge (SOC_{max})	1
Minimum electrode state of charge (SOC_{min})	0
Anodic Transfer Coefficient, α_a	0.5
Cathodic Transfer Coefficient, α_c	0.5
Electrolyte Reference Concentration	1 mol/m^3
Reaction Rate Coefficient (anodic, k_a and cathodic, k_c)	2×10^{-11} m/s
Initial Species (particles) Concentration	14870 mol/m^3
Maximum Solid Phase Concentration	26390 mol/m^3

Table I-3: Properties of $LiPF_6$ in 1:2 EC: DMC and p(VdF-HFP) (Polymer electrolyte).

Property	**Value**
Transport number	0.363
Activity dependence	0
Electrolyte salt concentration	1000 mol/m^3